RESEARCH ARTICLE

Wind stilling-reversal across Sweden: The impact of land-use and large-scale atmospheric circulation changes

Lorenzo Minola[1] | Heather Reese[2] | Hui-Wen Lai[1] |
Cesar Azorin-Molina[3] | Jose A. Guijarro[4] | Seok-Woo Son[5] | Deliang Chen[1]

[1]Regional Climate Group, Department of Earth Sciences, University of Gothenburg, Gothenburg, Sweden

[2]Department of Earth Sciences, University of Gothenburg, Gothenburg, Sweden

[3]Centro de Investigaciones sobre Desertificación, Consejo Superior de Investigaciones Científicas (CIDE-CSIC), Valencia, Spain

[4]State Meteorological Agency (AEMET), Delegation of the Balearic Islands, Palma de Mallorca, Spain

[5]School of Earth and Environmental Sciences, Seoul National University, Seoul, South Korea

Correspondence
Deliang Chen, Regional Climate Group, Department of Earth Sciences, University of Gothenburg, Gothenburg, Sweden.
Email: deliang@gvc.gu.se

Abstract

This study analyses for the first time the break in the stilling detected by previous research around 2010, with focus in Sweden using homogenized near-surface mean and gust wind speed observations for 1997–2019. During the recent past two decades, both mean and gust wind magnitude and frequency (exceeding the 90th percentile) underwent nonlinear changes, driven by the dominant winter variability. In particular, consistent with previous studies, the significant ($p < .05$) stilling ceased in 2003, followed by no clear trend afterwards. The detected stilling-reversal is linked to large-scale atmospheric circulation changes, in particular to the North Atlantic Oscillation for both mean and gust wind changes, and the intensity changes of extratropical cyclones passing across Sweden especially for wind gusts. Furthermore, in different wind change phases, the observed wind distribution did not vary uniformly for the various wind speed ranges; instead, strong winds drove most of the changes. In the same way, increases in gust winds are greater compared to changes in mean wind speed conditions. The stilling-reversal is also identified by the ERA5 reanalysis, where large-scale atmospheric circulation changes are captured. But the background slowdown detected in most stations does not appear in the ERA5 data as the observed increase in forest cover is not considered in the reanalysis. This study reveals that, in addition to the large-scale interannual variability, changes in surface roughness (e.g., changes in forest cover) contribute to the observed wind variability across Sweden.

KEYWORDS
ERA5, extratropical cyclones, mean and gust wind speeds, NAO, stilling-reversal phenomena, Sweden

1 | INTRODUCTION

By controlling the transfer of heat, moisture, energy and momentum between Earth's surface and atmosphere (Abhishek *et al.*, 2012), near-surface winds with their long-term changes have large environmental and socio-economic impacts. For instance, changes in surface mean winds can alter the energy production of wind farms

(Pryor *et al.*, 2005) and can affect agriculture productivity by regulating evaporation demand (Rayner, 2007). Surface winds also play a crucial role when it comes to the dispersion of air pollutants near emission sources such as urban traffic (Grundström *et al.*, 2011; Grundström *et al.*, 2015). Moreover, strong winds with their turbulent eddies can damage buildings and forests, increase aviation accidents, and thus represent a severe hazard to people, property and transportation (Achberger *et al.*, 2006; Suomi *et al.*, 2014). In particular, wind damages to trees can seriously threaten the national economy in Sweden, where the majority of forested land is used for the timber industry (Hannon Bradshaw, 2017). For example, the storm Gudrun in 2005, with its strong and sudden gusts, fell about 75 million m^3 trees in Sweden alone, which equals the normal annual harvest of the whole country (Haanpää *et al.*, 2007). Falling trees can further damage power supplies, telecommunication networks, roads and railways; even human fatalities can occur (Swedish Commission on Climate and Vulnerability, 2007).

During the last few decades, various studies have used in-situ observations to investigate multidecadal changes in near-surface wind speed, revealing a general slowdown in terrestrial winds, termed "stilling" by Roderick *et al.* (2007). Such mean wind speed decrease was observed mainly over land in most northern mid-latitude regions in the last ∼30–50 years (McVicar *et al.*, 2012; Zhang *et al.*, 2019), differing from the increase in surface wind speed over large parts of the oceans, especially in the Southern Hemisphere (Tokinaga and Xie, 2011; Young and Ribal, 2019). However, the mean surface wind speed in the Northern Hemisphere has shown a reversal in its decline during recent years (Kim and Paik, 2015; Azorin-Molina *et al.*, 2018a; Zhang and Wang, 2020). Such a break in the terrestrial stilling became prominent since around 2010, especially over Europe, East Asia and North America (Zeng *et al.*, 2019).

Different possible causes of the origin of the ocean wind increase, terrestrial wind stilling and its reversal have been proposed. The terrestrial wind stilling is partly attributed to the increase in surface roughness such as land-use changes, forest growth and urbanization (Vautard *et al.*, 2010). However, land greening alone cannot explain the magnitude of the terrestrial wind reduction (Zeng *et al.*, 2018); for this reason, several studies have proposed large-scale atmospheric circulation as a key driver in modulating observed wind changes (Wu *et al.*, 2018; Zeng *et al.*, 2019). In fact, air temperature changes in a warming climate can affect surface pressure gradients and therefore circulation patterns (Lin *et al.*, 2013). For example, the reversal in the terrestrial mean wind slowdown has been linked to phase changes in the North Atlantic Oscillation (NAO; Azorin-Molina *et al.*, 2018a) and the Pacific Decadal Oscillation (Zeng

et al., 2019). It is important to mention that artificial issues related for example to the ageing of measuring instruments can sometimes contribute to the observed wind speed slowdown (Azorin-Molina *et al.*, 2018b).

Given the large impact of winds across Sweden, multidecadal variability in observed mean wind speed was previously investigated in this region by Minola *et al.* (2016). Long-term trends over 1956–2013 show an overall statistically significant decrease over Sweden. The magnitude of the decline is in line with previous studies in nearby regions or similar latitude regions, but strong seasonal differences were also found (i.e., a large decline in spring, summer and autumn; but a weak increase in winter). Such differences in seasonal trends reveal the strong influence of large-scale atmospheric circulation, in particular the importance of the NAO circulation pattern in modulating winter wind speed variability.

When it comes to wind extremes such as wind gusts, it is still unclear how they can change in relation to the mean wind due to the possible changes in wind speed distribution (Wu *et al.*, 2018). The main reason limiting extreme wind variability research is that there are various artefacts which can affect the reliability of extreme wind observations (e.g., station relocations, anemometer height changes, etc.; Azorin-Molina *et al.*, 2014). More importantly, systematic measurements of extreme winds are often lacking or available only in the last few decades (Minola *et al.*, 2021). For example, in Sweden, widespread gust wind measurements were recorded only since the end of the 1990s and no study before has been able to evaluate changes in observed wind gusts in this region.

As wind observations are often not available or reliable, alternative datasets can be used instead to explore surface wind variability. Reanalysis datasets, by combining observations and models, generate consistent wind time series at a complete spatial coverage and for this reason can potentially be used for such research (Dee *et al.*, 2011). Before using a reanalysis product for assessing wind changes, its capability to realistically represent surface winds must be evaluated against in-situ observations since reanalysis dataset performance is strongly dependent on the selected region and the considered time period (Ramon *et al.*, 2019; Wohland *et al.*, 2019; Yu *et al.*, 2019; Miao *et al.*, 2020). Among the various reanalyses available nowadays, ERA5 (Hersbach *et al.*, 2018) is the new promising reanalysis dataset produced by the European Center for Medium-Range Weather Forecasts (ECMWF). Its ability to represent both mean and gust wind speed climatology across Sweden was tested by Minola *et al.* (2020) for the time period 2013–2017, but the ERA5 potential for capturing long-term wind variability was not evaluated.

Given the recent break in the terrestrial wind decline in northern mid-latitude regions, this study explores the

latest (1997–2019) changes in surface wind variability across Sweden to investigate if a stilling-reversal is also detected at such high-latitudes. This study focuses on the recent past which was only partly covered by Minola *et al.* (2016) and when near-surface wind gust measurements are available. In this way, decadal variability of observed wind gusts is explored for the first time across Sweden and its relationship with mean wind speed changes is assessed. The plausible reasons behind the observed variability are also examined by evaluating the changes in large-scale atmospheric circulation (i.e., NAO) and synoptic weather systems (i.e., extratropical cyclones) which could be responsible for the stilling-reversal. The ability of the new ERA5 reanalysis product to represent surface wind variability across Sweden is also tested. By comparing ERA5 wind changes with the observations, additional causes (e.g., increase in surface roughness) behind the observed wind variability are identified.

2 | DATA

2.1 | Wind observations

For weather monitoring and forecasting, measuring stations record near-surface mean wind speed (hereafter, WS), defined as the average wind speed over the last 10 min in a specified time interval (WMO, 2014). They also measure wind gust (hereafter, WG), i.e., the maximum 3 s wind speed over the last hour (Beljaars, 1987). By definition, WG measurements can capture with its short average time the sudden and brief increase in wind speed, which is important when considering buildings' wind-loading standards (Kwon and Kareem, 2014). Hourly WS and WG measurements across Sweden are provided by the Swedish Meteorological and Hydrological Institute (SMHI). They can be retrieved online at the SMHI open data page (https://www.smhi.se/data/utforskaren-oppna-data/; last accessed May 6, 2021). Following the World Meteorological Organization's (WMO) guidelines, SMHI measures WS at 10 m above ground as the average wind over a 10 min interval for each hour (Minola *et al.*, 2020). WG is defined as the maximum 2 s gust recorded in the last hour at 10 m height. Note that this averaging time differs by 1 s from the standard 3 s averaging time recommended by WMO (Beljaars, 1987). SMHI calculates wind averages as vector values and this way of averaging has been the same since 1977 (S. Tainamo, personal communication, April 19, 2021).

In 1996, SMHI started to install automatic weather stations across the country (Wern and Bärring, 2009), and it is only since then that hourly WS measurements were systematically recorded and hourly WG observations became available (Minola *et al.*, 2021). Thus, using hourly observations,

daily wind series are prepared for the longest available time period of 1996–2019. Daily average mean wind speed series (hereafter, DAWS) are calculated as the average WS recorded in 24 hr. It is computed only for those days which have more than 12 hourly WS observations; otherwise, the day is labelled as a missing observation. The daily peak wind gust series (hereafter, DPWG) are constructed with the highest WG recorded in 24 hr (Azorin-Molina *et al.*, 2016). If there are less than 19 hourly WG observations for a given day, DPWG measurement is recorded as a missing value. Among a total of 168 weather stations in Sweden, DAWS and DPWG series from 100 stations are examined in this study as they (a) were evenly distributed across the whole of Sweden; and (b) covered the longest-available time period (1997–2019) with less than ~1.5 years (i.e., 547 days) of missing observations. Note that year 1996 is excluded because most of the stations have a long period of missing observations during that year. The spatial distribution of the selected 100 weather stations is shown in Figure 1.

Various types of non-climatic factors, such as station relocations and anemometer height and type changes (Wan *et al.*, 2010), can create artificial shifts in near-surface wind series, making those data unrepresentative of the actual climate variations over time (Aguilar *et al.*, 2003). For this reason, a homogenization protocol is applied to correct the observed wind series from those possible biases. This study uses *Climatol* (Guijarro, 2017) to perform homogenization and missing data infilling on the raw 100 DAWS and DPWG series. A detailed description of the homogenization approach adopted in this study can be found in Azorin-Molina *et al.* (2016), Zhang *et al.* (2020) and Minola *et al.* (2021).

2.2 | ERA5 dataset

This study uses wind outputs of the ERA5 reanalysis, which is the latest reanalysis product of ECMWF (Hersbach *et al.*, 2018). ERA5 delivers hourly outputs of both WS and WG at a horizontal grid spacing of approximately 31 km. Notice that ERA5, like other modern reanalyses, does not assimilate near-surface wind observations over land because they cannot be fully interpreted by the data assimilation system (Dee *et al.*, 2011). Instead, terrestrial vertical wind profiles from satellites, radio- and aircraft-sondes are included. Minola *et al.* (2020) compared ERA5 (and ERA-Interim) WS and WG outputs with observations for the time period 2013–2017. They showed the improvements made by ERA5 in comparison with its predecessor ERA-Interim.

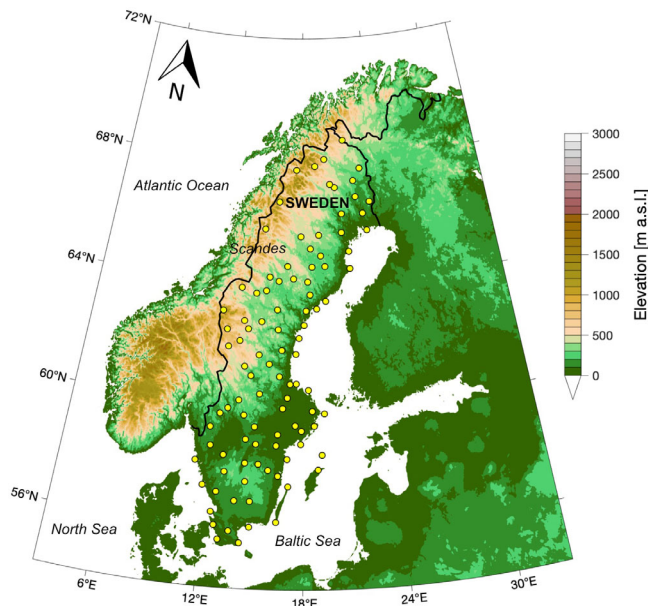Hourly wind data of ERA5 are downloaded from the Copernicus website (https://cds.climate.copernicus.eu/

FIGURE 1 Elevation map of Sweden (and surrounding) with the location of the 100 weather stations used in this study (circles) [Colour figure can be viewed at wileyonlinelibrary.com]

cdsapp#!/dataset/reanalysis-era5-single-levels?tab=overview; last accessed May 6, 2021). By using these hourly WS and WG outputs, DAWS and DPWG series are also constructed for ERA5 in the same way they are calculated for observation. In this study, following Minola *et al.* (2020), each observed wind series is compared with the wind series from the ERA5 grid point closest to the weather stations, under the assumption that this closest series matches the observed one better than any other more distant grid point.

2.3 | NAO index

Given the strong control of the NAO teleconnection pattern on the winter climate in the Northern Hemisphere (Wallace and Gutzler, 1981; Hurrell, 1995) and Sweden (Hurrell and van Loon, 1997; Chen and Hellström, 1999; Linderholm *et al.*, 2011; Minola *et al.*, 2016), the influence of large-scale atmospheric circulation on wind stilling-reversal is investigated by using a NAO index. As NAO describes the relative changes in pressure between the Icelandic low-pressure region and the relatively high-pressure centred over the Azores islands (NOAA, 2012), the NAO index is defined as the normalized sea-level pressure difference between Gibraltar and southwestern Iceland (e.g., Reykjavik) (Jones *et al.*, 1997). The NAO index used in this study is obtained from the Climatic Research Unit, University of East Anglia (https://crudata.uea.ac.uk/cru/data/nao; last accessed May 6, 2021).

2.4 | Aerial photography and Lidar data

To identify possible changes in surface roughness (i.e., forest), ortho-corrected colour-infrared aerial photographs (i.e., orthophotos) from 1998 to 2018 are used, with one image selected per 3-year time interval (1998–2000; 2001–2003; ...; 2016–2018) for a variety of sites ($n = 13$). The orthophotos have a variable grid cell size. For instance, images from 1998 to 2000 have 1 m grid cells, while images from 2001 to 2008 and those since 2009 have 50 and 25 cm grid cell size, respectively. Aerial photographs are acquired by the Swedish Mapping, Cadastral and Land Registration Authority (Lantmäteriet, https://www.lantmateriet.se/; last accessed May 6, 2021) approximately every other year over forested areas in southern Sweden, and on a 5-year cycle in northern inland Sweden. In exceptions where an orthophoto is not available within a 3-year period, Landsat-7 ETM+ optical satellite data are downloaded from the US Geological Survey (https://earthexplorer.usgs.gov/; last accessed May 6, 2021) to distinguish between forested and non-forested areas with the 15 m grid cell resolution panchromatic band. Data on forest height and density estimates for the years 2010–2012 created from Sweden's national airborne Lidar dataset are available from the National Land Cover data (https://www.naturvardsverket.se/Sa-mar-miljon/Kartor/Nationella-Marktackedata-NMD/; last accessed May 6, 2021). In addition, forest biomass for the years 2000, 2005, 2010 and 2015 are referenced using SLU forest data (https://www.slu.se/centrumbildningar-och-projekt/riksskogstaxeringen/statistik-om-skog/slu-skogskarta/; last accessed May 6, 2021).

3 | METHODS

3.1 | Wind series

Following Azorin-Molina *et al.* (2021), decadal variability is investigated for both the DAWS and DPWG magnitude (in m s^{-1}), and for the number of days (hereafter, frequency; in days) of DAWS and DPWG events exceeding the 90th percentile (Vose *et al.*, 2014). Frequency series are calculated for each station series. For example, to calculate the spring frequency series of a given station, first the overall 90th percentile for all spring (i.e., March–April–May) days during 1997–2019 is determined; then, the number of spring days exceeding this value in each year is counted. Therefore, if the magnitude represents the average wind behaviour, the frequency looks at the occurrence of extreme wind events (i.e., the upper tail of the wind distribution) (Azorin-Molina *et al.*, 2021). Analyses are performed at annual and seasonal time steps, using boreal seasons: winter (December–February),

spring (March–May), Summer (June–August) and autumn (September–November).

The decadal variability is also evaluated for different wind speed categories, expressed as percentiles (5th, 10th, 25th, 75th, 90th and 95th). This enables us to evaluate the relative importance of light and strong wind changes. Furthermore, to explore the relationship between mean and gust wind speeds, the gust factor (G) is also computed for each day by dividing the measured DPWG with the recorded DAWS (Suomi et al., 2014):

$$G = \frac{\text{DPWG}}{\text{DAWS}} \tag{1}$$

3.2 | Trend analysis

Linear trends are calculated through a linear fit between time (independent variable) and winds (dependent variable). The magnitude of the trend is defined by the slope of the linear trend and is estimated with the nonparametric Sen's method (Gilbert, 1987). The significance of the trend is calculated by applying the modified Kendall trend test to consider the effect of statistically significant autocorrelation (Hamed and Ramachandra Rao, 1998). Trends are reported at three different significance categories following Azorin-Molina et al. (2014): (a) significant at $p < .05$; (b) significant at $p < .10$; and (c) non-significant at $p > .10$. In this way, it is possible to highlight the significance range of the trend, instead of just focusing on whether it is significant according to an arbitrary p level. To show the different time period dominated by increase or decline in wind, running trends are computed for varying window lengths from 5 (e.g., 1997–2001) to 23 years (e.g., 1997–2019). In addition to linear and running trends, a Gaussian-weighted average filter over 10-year windows is also applied to the investigated wind series to more clearly illustrate the lower-frequency modes of variability of winds. On top of the trend analyses, the degree of association (or linear relationship) between two series is measured with the Pearson's correlation coefficient (r; Gibbons and Chakraborti, 2011) and its significance is expressed at the $p < .05$ level.

3.3 | Extratropical cyclone tracking

To track extratropical cyclones, the most commonly used tracking features are mean sea level pressure (MSLP) or lower-tropospheric relative vorticity (e.g., Hoskins and Hodges, 2002; Hewson and Titley, 2010). Relative vorticity focuses more on a smaller synoptic-scale and is used to detect cyclones at an earlier stage, while MSLP is more dominated by large-scale features and smooths smaller-scale features that are of interest (Hodges et al., 2003). Many cyclone tracking methods and algorithms have been developed and applied to analyse cyclone climatology, future changes in cyclone characteristics, and links between cyclones and dynamic/thermodynamic processes (Neu et al., 2013).

In this study, we apply a Lagrangian cyclone tracking algorithm developed by Hodges (1994, 1995, 1996), which is based on objective methods and tracks time sequences of meteorological variables, such as geopotential, relative vorticity and MSLP. This algorithm has been applied to study climatic variability of mid-latitude cyclones in global and regional studies (e.g., Hoskins and Hodges, 2002; Grise et al., 2013; Baker et al., 2019; Lee et al., 2020). The tracking algorithm is applied to ERA-Interim from 1979 to 2018 with a 6-hr temporal resolution. To focus on large-scale flows where extratropical cyclones are embedded, MSLP filtered at a wavenumber range from 5 to 63 ($\approx$ 180 km) is chosen as the tracking feature. Following Lee et al. (2020), we also filter out the cyclones that are initialized at the latitude below 25°N, have a lifetime shorter than 2 days, or travel less than 1,000 km. Among the detected cyclones, the cyclones that pass across Sweden (within 55°N–69°N and 10°E–25°E), assuming an influence radius of 555 km from the centre of the cyclones, are considered in this study. Both the cyclone density (in number) and mean intensity (in hPa) are examined. Since cyclone influence is strongest in the proximity of the areas where it passes, DAWS and DPWG for a given weather station are compared only with the cyclone statistics of the closest grid point in the MSLP field.

3.4 | Quantification of vegetation changes

Before considering surface roughness changes in the proximity of each weather station, we characterize the geographic characteristics around each station using Google Maps (https://www.google.com/maps/; last accessed May 6, 2021). The weather stations are classified according to common features (detected within a 1 km distance) as being (a) urban, (b) on islands, (c) coastal regions, (d) near airports, (e) in mountains, (f) inland with nearby cultivated fields, (g) inland with nearby forest, (h) inland with mix of cultivated fields and forests nearby, or (i) in proximity to a lake or river. Thirteen weather stations are selected representing at least one of the different classes. For each of the 13 stations, seven orthophotos from the time period 1998–2018 are

used, with one image per three-year period starting from 1998. Within a 1 km × 1 km frame centred on the weather station, forest versus non-forest is manually digitized over the orthophotos at a visual scale of 1:6,000. Forest is defined as tree-covered regions with at least 10% canopy cover and tree heights of at least 5 m at a minimum mapping unit of 400 m². Canopy cover is judged visually and tree heights are determined from image shadows as well as reference to tree height, density and biomass from SLU forest data and National Land Cover data.

Starting with the most recent orthophoto (2016–2018), forested areas are delineated in a vector coverage and forest area is calculated (in m²). The initial vector file is copied to serve as a starting point for the previous 3-year period and the existing polygons are modified to represent forested areas for that time period. This process is repeated until the earliest time period (1998–2000) is reached. For the case of the urban site, Malmö, changes in buildings over 5 m in height near the weather station are included in the surface roughness statistics.

4 | RESULTS

4.1 | DAWS and DPWG variability

Figure 2 shows the mean (i.e., average over all stations) annual DAWS and DPWG variabilities during 1997–2019. In all series, four phases of wind changes are identified: (a) clear slowdown during 1997–2003, (b) stabilization from 2003 to 2010, (c) slight recovery during 2010–2014 and (d) start of a new slowdown since 2014. This temporal pattern, observed at an annual scale, is mostly driven by winter variability in which those four phases of changes are more evident (Figure 3). In summer, wind conditions do not vary much for the whole analysis period of 1997–2019. The four phases become distinct when looking at running trends. Figure 4 summarizes the running trends detected for annual DAWS series during 1997–2019. A large number of stations (more than 50%) shows significant declines until 2003, but afterwards different periods of increasing and
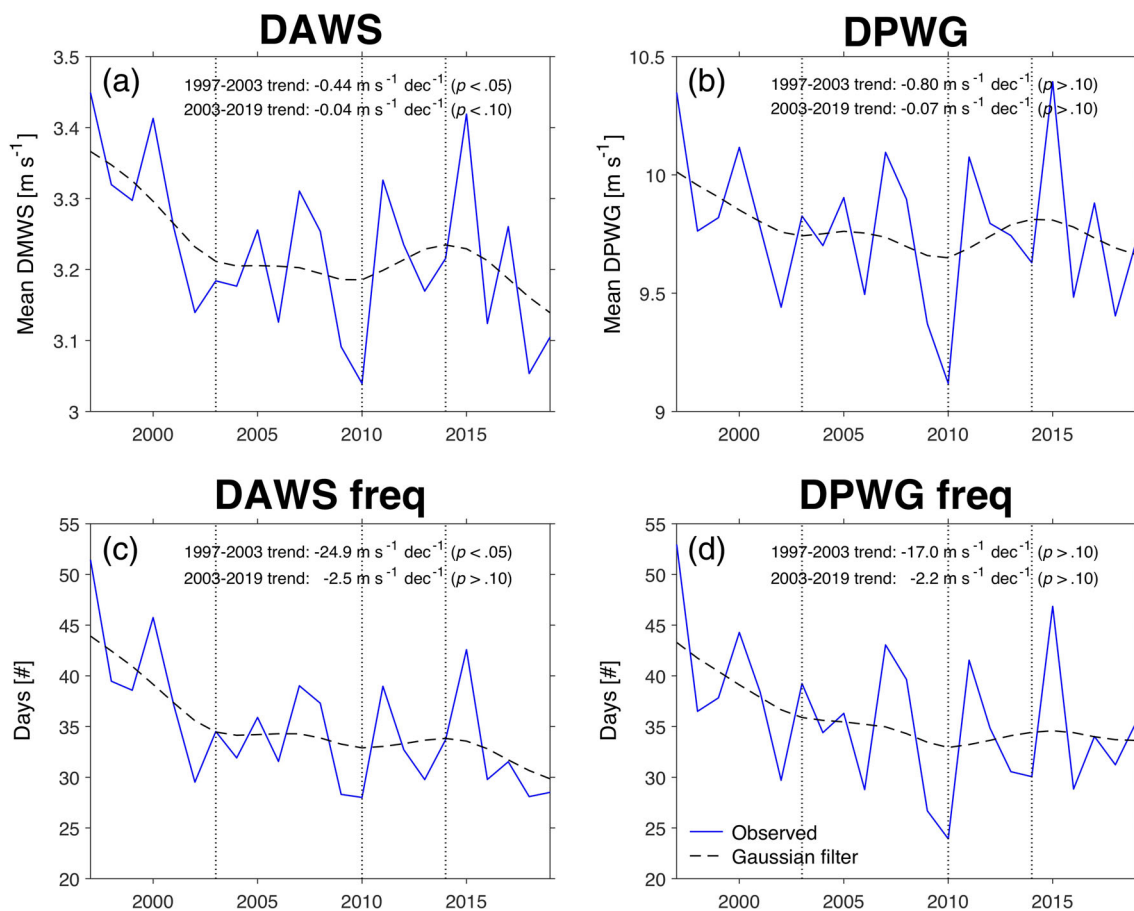

FIGURE 2 Series of mean (i.e., average over all stations across Sweden) annual (a) DAWS, (b) DPWG, (c) DAWS frequency and (d) DPWG frequency from 1997 to 2019. The low-frequency variability is shown with the black dashed lines of the applied Gaussian-weighted average (10-year window) [Colour figure can be viewed at wileyonlinelibrary.com]
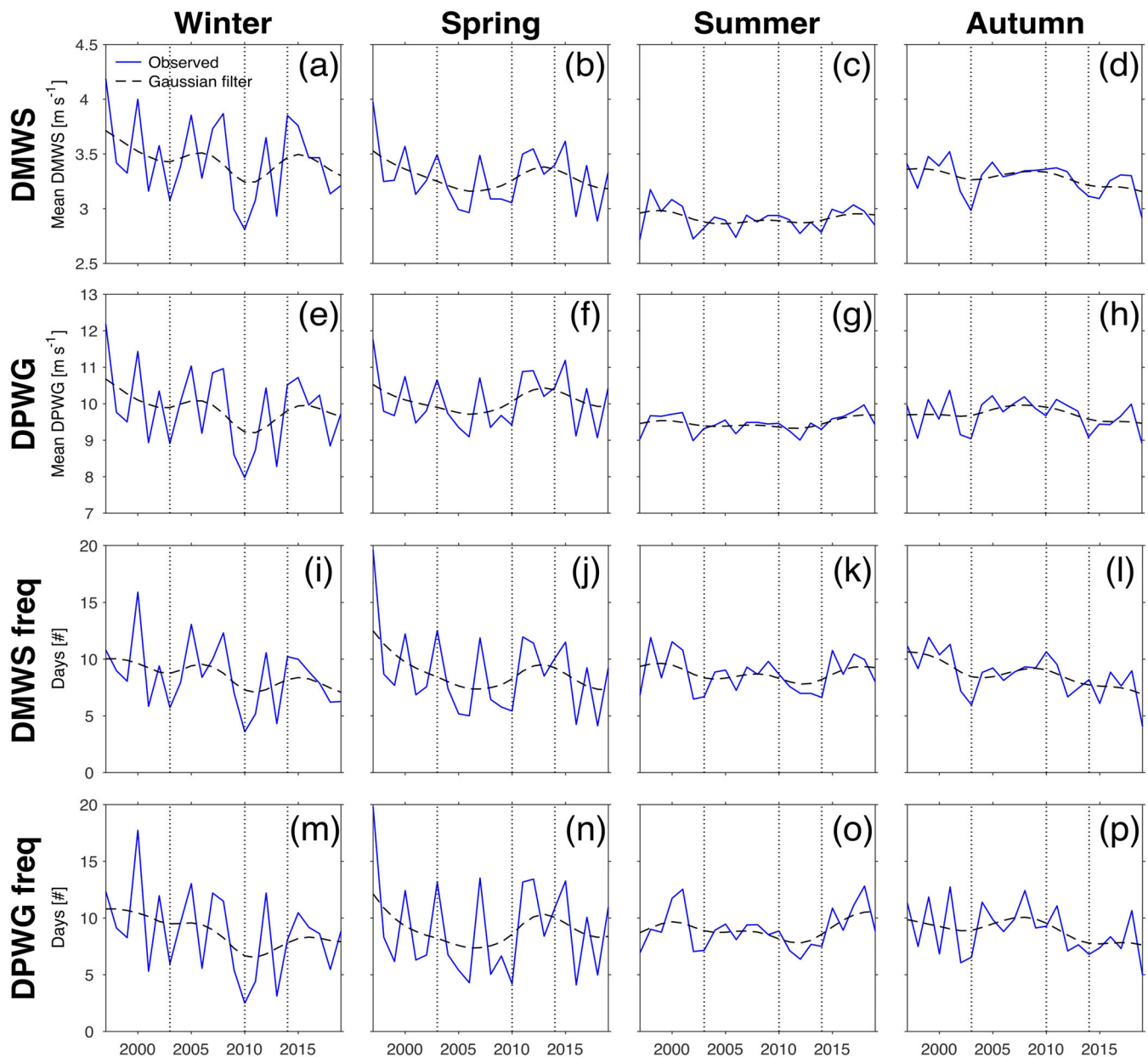
FIGURE 3 Series of mean (i.e., average over all stations across Sweden) seasonal DAWS (first row), DPWG (second row), DAWS frequency (third row), and DPWG frequency (fourth row) from 1997 to 2019. The low-frequency variability is shown with the black dashed lines of the applied Gaussian-weighted average filter (10-year window) [Colour figure can be viewed at wileyonlinelibrary.com]

decreasing of DAWS are detected (with significant trends becoming less frequent).

When 1997–2003 trends are compared with the ones for 2003–2019, strong negative trends of DAWS, which are statistically significant at $p < .05$, are found before 2003 (see also Figure 2). After 2003, mean DAWS and DAWS frequency trends have lower magnitude and become significant only at $p < .10$ or even insignificant ($p > .10$). Both mean DPWG and DPWG frequency trends exhibit insignificant trends ($p > .10$) even if the slowdown is also much greater before 2003: the higher

interannual variance in the gust series can be the reason behind such insignificance (Weatherhead et al., 1998).

The observed 1997–2019 variability detected here is in line with the 1956–2013 multidecadal WS changes investigated by Minola et al. (2016) (Figure 5), even though this previous study used only 23 weather stations and homogenization was carried on a monthly basis (which could explain mean WS bias of ∼0.4 m s^{-1} in the common period). Among others, the slowdown during 1997–2003 comes from the longer wind decline observed since 1990. When looking at the running trends (Figure 6),
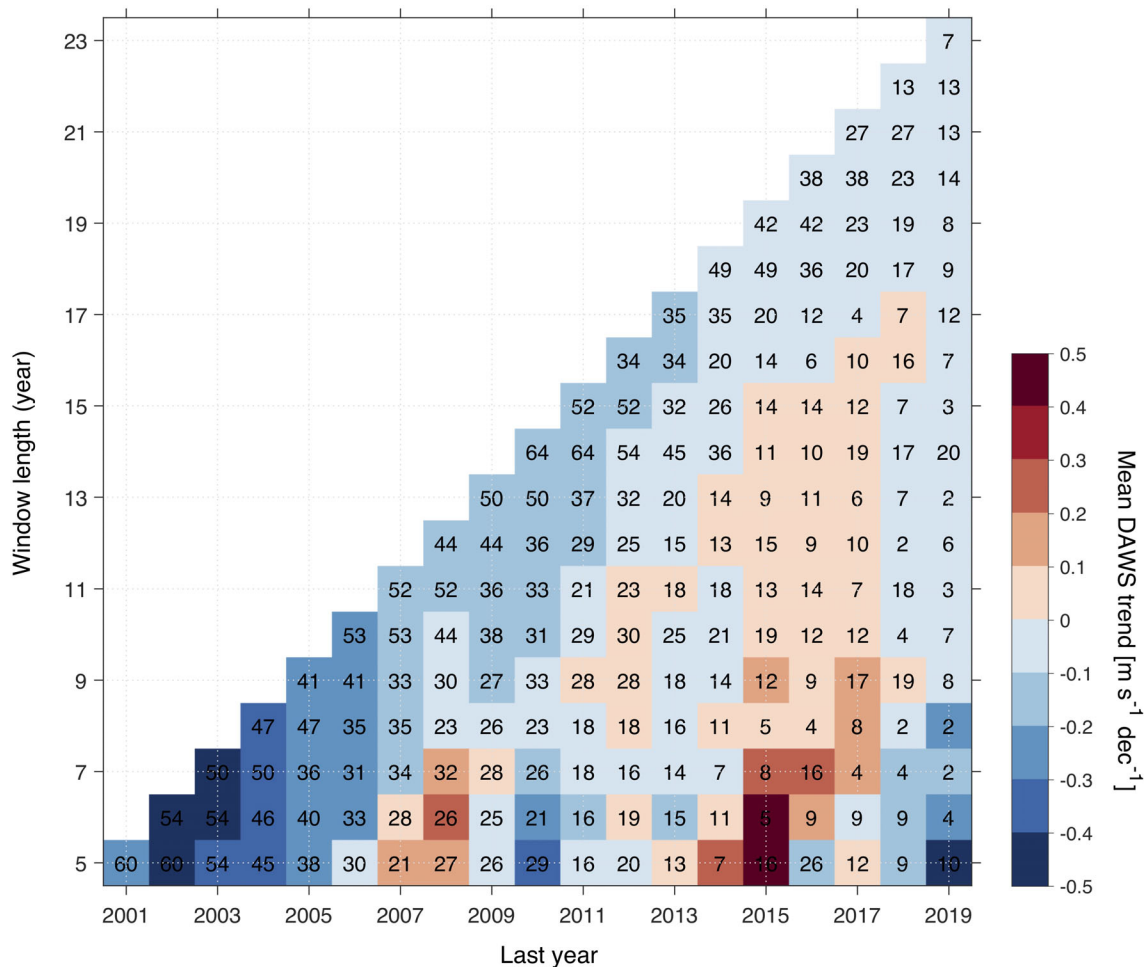
FIGURE 4 Summary of running trends of annual DAWS in Sweden for 1997–2019. Each square shows the mean trends for all 100 weather stations. The reported number is the percentage of stations displaying significant trend ($p < .1$) for the same sign of the mean trend (i.e., if the mean positive trend is positive, the number shows the percentage of stations displaying significant positive trend) [Colour figure can be viewed at wileyonlinelibrary.com]

1956–2013 WS series show significant ($p < .05$) decreasing trends during 1990–2003, which are detected (also at $p < .05$) in DAWS series during the 1997–2003 time period. After that, wind series undergo periods of light increase and decrease, and no clear trend can be detected. Even though an overall WS decline was observed during 1956–2013 (Minola *et al.*, 2016), no evident trend is detected since around 2003 and a recovery from previous years' slowdown is observed. To conclude, it is obvious that wind series pass through different phases of change, not only during 1997–2019, but since 1956.

4.2 | DAWS–DPWG relationship

Figures 2 and 3 show that observed DAWS and DPWG display similar annual and seasonal variabilities in the last two decades, showing the same four phases of

changes as described in Section 4.1. This indicates that time periods with stronger mean winds occur together with stronger gusts as well. In the same way, DAWS and DPWG frequencies have similar temporal patterns: that is, years having days with stronger than usual mean winds are also the years having days characterized by stronger gusts. Thus, when looking at the correlation between DAWS and DPWG series (Table 1), high correlation coefficients (greater than ∼0.8) are found for both annual and seasonal variabilities, with all stations displaying significant correlation at $p < .05$. A slightly lower correlation is displayed during summer compared to winter, most probably due to the occurrence of deep convective and mesoscale convective systems at the origin of convective gusts (Jeong *et al.*, 2011; Punkka and Bister, 2015).

To further investigate the relationship between mean and gust wind speed, Figure 7 plots the annual and
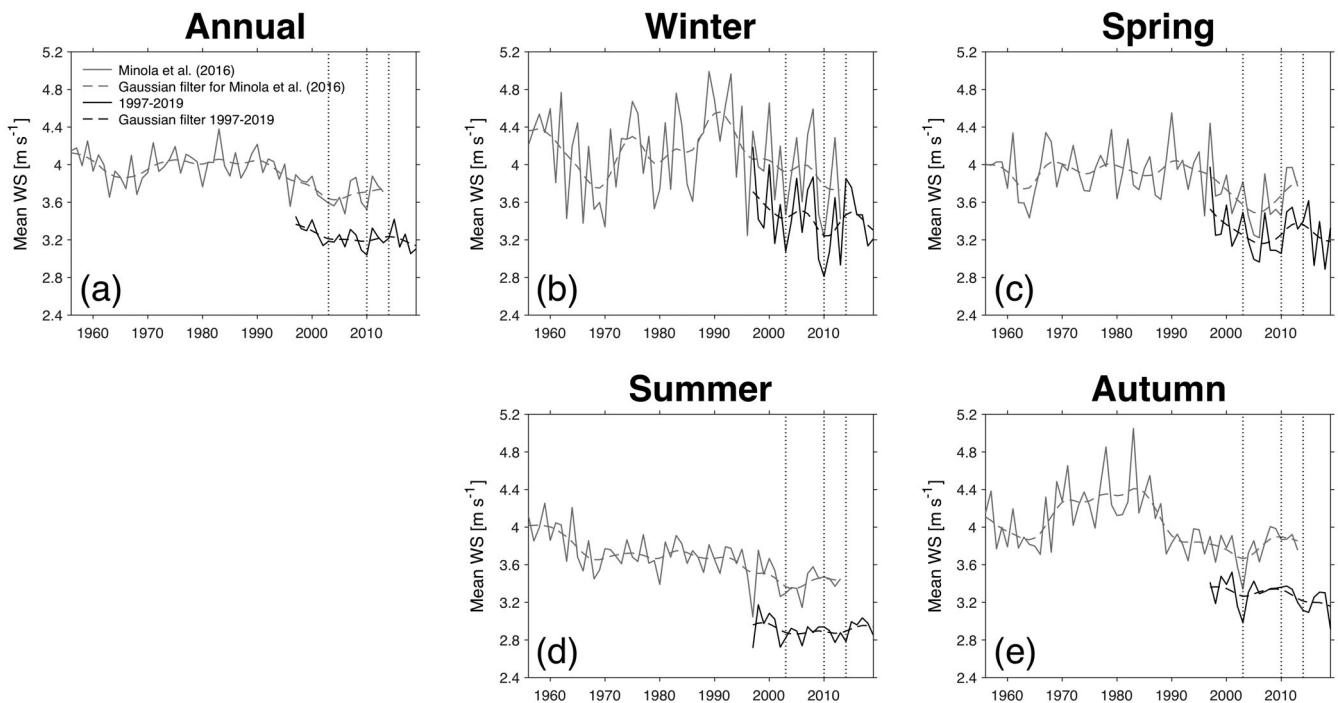
FIGURE 5 Series of mean (i.e., average over all stations across Sweden) annual and seasonal WS during 1997–2019 (black line) and during 1956–2013 (from Minola *et al.*, 2016; grey line). The low-frequency variability is shown with the dashed lines of the applied Gaussian-weighted average filter (10-year window)

seasonal variabilities of the gust factor (*G*) during 1997–2019. The four-phases temporal pattern is also captured, in particular over winter, but with an opposite sign. For example, the 1997–2003 DAWS and DPWG slowdown period is a strengthening phase in *G*. Given the gust factor definition, this indicates that gust wind changes are stronger than the ones in mean wind speed. When DPWG changes, it increases or decreases much greater than DAWS does. This is also seen in other percentiles. When plotting the standard deviation of annual and seasonal wind ranges (Figure 8), higher percentiles of both DAWS and DPWG show a larger dispersion, especially in winter. This result indicates that wind changes depend on wind speeds and, when the wind distribution changes, it does not change evenly. In particular, stronger winds (higher percentiles) undergo stronger increases or decreases compared to weaker winds (lower percentiles). In addition, the wind distribution ends up having a wider range of values during increasing phases and a narrower range during slowdown phases.

4.3 | NAO index and extratropical cyclone influence

To explain the four phases of wind changes and the stilling-reversal, we look here at the impact of large-scale atmospheric circulation, in particular the NAO. The NAO index correlates well with all wind series during winter, when most stations show significant positive correlation coefficients at $p < .05$ (Table 2). Consistent with the observed wind changes, the winter NAO index underwent four different change phases during 1997–2019 (Figure 9): that is, (1) clear negative trend during 1997–2003, (2) weak negative trend during 2003–2010, (3) strong positive trend during 2010–2014 and (4) negative trend again since 2014/2015. Note that year 2010 is when the lowest NAO index is recorded (Buchan *et al.*, 2014), which also corresponds to the year of the lowest DAWS and DPWG values. Therefore, the reported decadal variability of wind speed across Sweden, including the recent stilling-reversal since 2003, can be largely explained by the NAO index.

The impact of synoptic weather systems is also investigated by looking at the influence of extratropical cyclones on the observed wind variability. Table 3 shows the correlation coefficients between the various wind series and cyclone statistics during 1997–2018. The cyclone frequency correlates well with DPWG frequency, with 67 stations showing significant positive correlations at $p < .05$. The impact of cyclone intensity also appears in all wind series during winter, especially with a high correlation for DPWG frequency. More than 70% of the
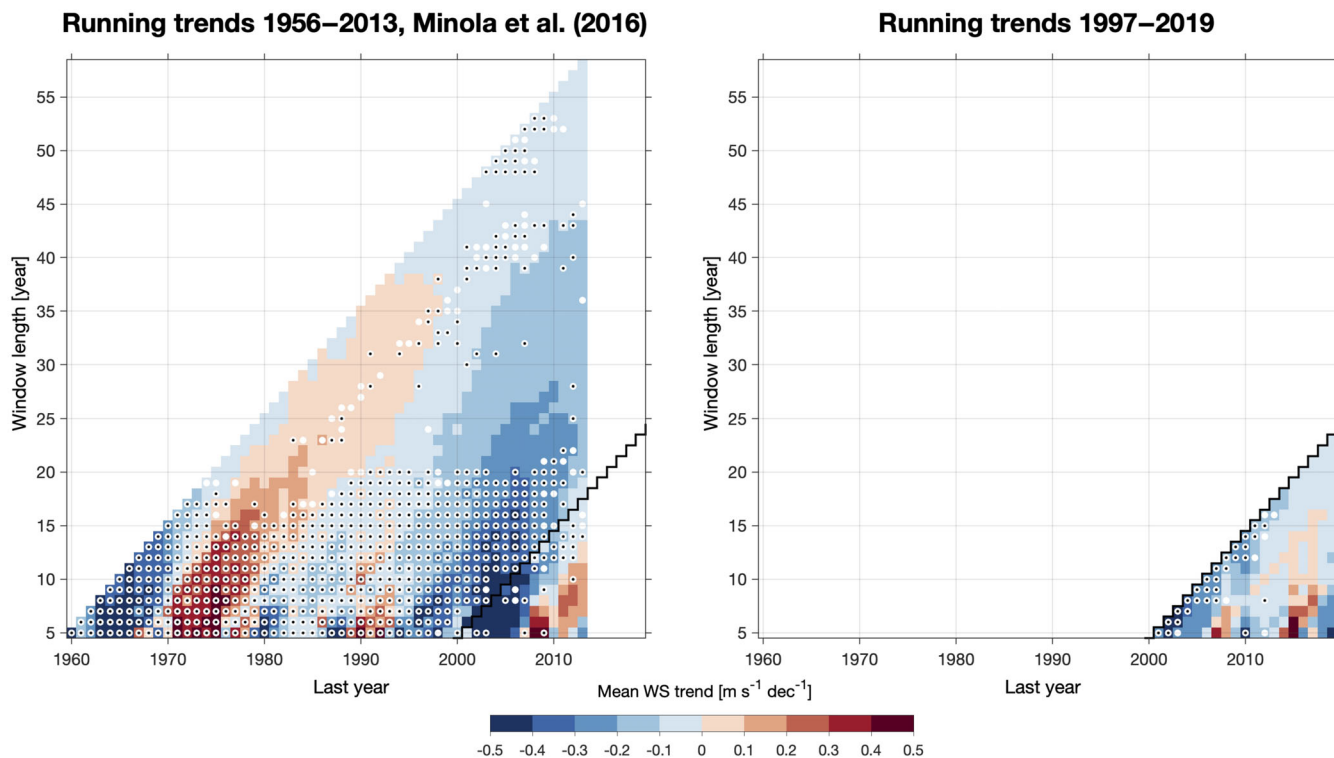
FIGURE 6 Running trends of mean (i.e., average over all stations across Sweden) annual WS for (a) 1956–2013 (from Minola *et al.*, 2016), and (b) 1997–2019 (left). Square with a white circle in the middle represents trends significant at $p < .1$; square with a white circle and a black dot in the middle represents trends significant at $p < .05$ [Colour figure can be viewed at wileyonlinelibrary.com]

	Pearson's correlation coefficient - DAWS vs. DPWG				
	Mean	**Positive**	**Positive $p < .05$**	**Negative**	**Negative $p < .05$**
Annual	0.83	100	99% (99)	0	0% (0)
Winter	0.93	100	100% (100)	0	0% (0)
Spring	0.90	100	100% (100)	0	0% (0)
Summer	0.79	100	99% (99)	0	0% (0)
Autumn	0.82	100	100% (100)	0	0% (0)

TABLE 1 Annual and seasonal relative frequency (%) and number of stations in parentheses showing non-significant and significant ($p < .05$) positive and negative Pearson's correlation coefficient between DAWS and DPWG series for 1997–2019. It is also reported the mean Pearson's correlation coefficient value

Notes: Relative frequencies are calculated with respect to the total number of stations showing positive or negative correlation.

stations show significant negative correlation at $p < .05$ between DPWG frequency and cyclone intensity. Note that as intensity refers to SLP anomaly, negative correlation indicates a stronger wind when a stronger cyclone passes. The higher and significant (at $p < .05$) correlation values during winter are observed all across the country, except at higher latitudes above ~65°N (Figure 10a). When only weather stations in which wind series are significantly correlated with cyclone frequency at $p < .05$ are considered, their regional-mean DPWG in winter is clearly negatively correlated with the cyclone intensity, that is, the winters with stronger cyclones are the winters when stronger DPWGs are recorded (Figure 10b). Thus, when considering

the impact of extratropical cyclones hitting Sweden, their intensity largely affects the wind strength during winter, especially when it comes to the occurrence of strong wind gusts. Likewise, cyclone frequency impacts the occurrence of days of stronger than usual gusts. In view of the different wind phase changes, extratropical cyclones could have also played a key role in the wind stilling-reversal detected across Sweden (in particular when it comes to wind gusts). Notice that extratropical cyclones are influenced by the background airflow, which is modulated by the NAO (Keim *et al.*, 2004). Indeed, NAO index correlates well with winter cyclone statistics during 1979–2018: for frequency, mean correlation is 0.49, significant ($p < .05$) for 87% of the
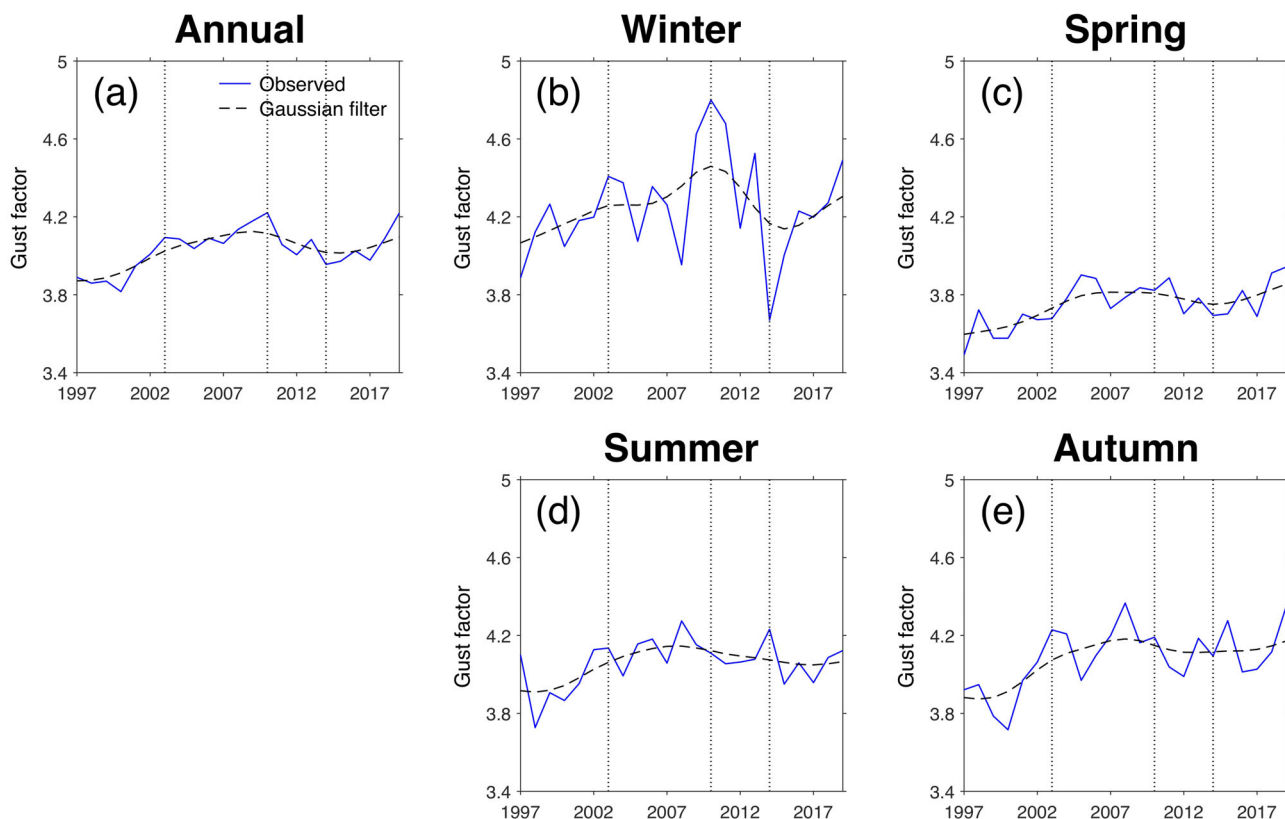
FIGURE 7 Series of mean (i.e., average over all stations across Sweden) annual and seasonal gust factor for 1997–2019. The low-frequency variability is shown with the black dashed lines of the applied Gaussian-weighted average (10-year window) [Colour figure can be viewed at wileyonlinelibrary.com]
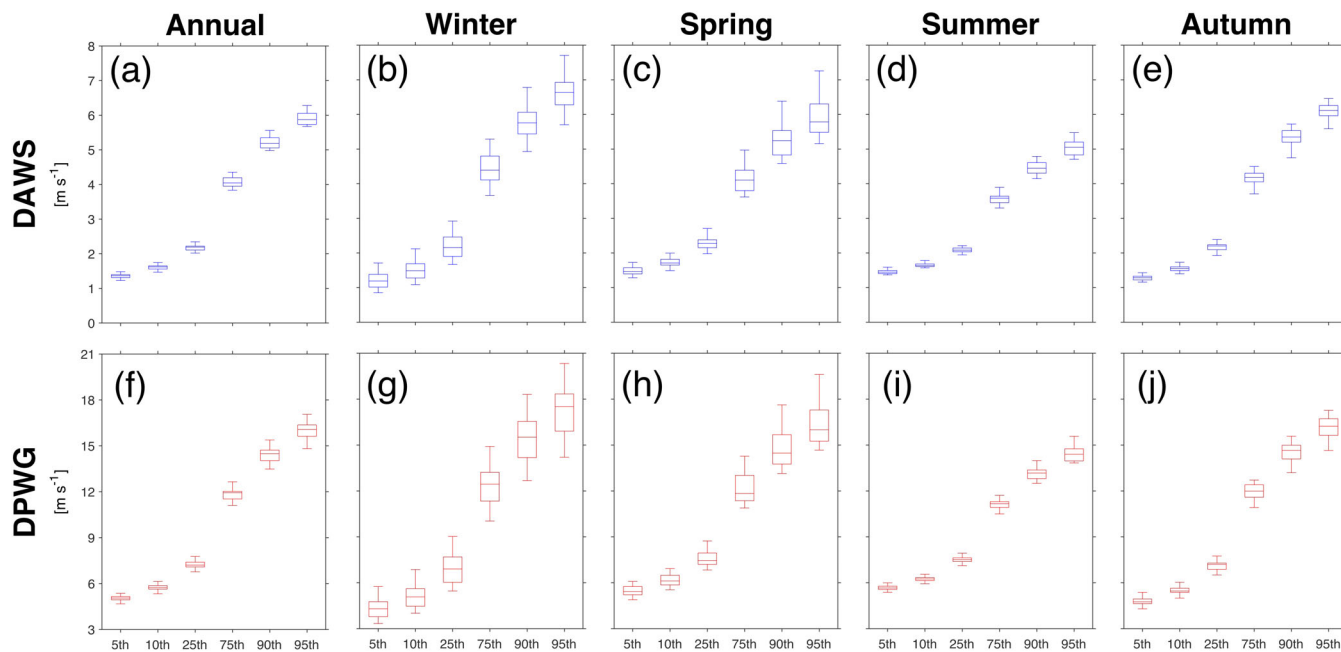

FIGURE 8 Boxplot of mean (i.e., average over all stations across Sweden) annual and seasonal DAWS (top row) and DPWG (bottom row) for different wind ranges expressed as percentiles during 1997–2019. On each box, the central mark indicates the median, and the bottom and top edges of the box indicate the 25th and 75th percentiles, respectively. The whiskers extend to the most extreme data points not considered outliers, that is, to approximately +/−2.7σ [Colour figure can be viewed at wileyonlinelibrary.com]

TABLE 2 Annual and seasonal relative frequency (%) and number of stations in parentheses showing non-significant and significant ($p < .05$) positive and negative Pearson's correlation coefficient between NAO index and (i) DAWS, (ii) DPWG, (iii) DAWS frequency, and (iv) DPWG frequency series for 1997–2019. It is also reported the mean Pearson's correlation coefficient value

		Pearson's correlation coefficient vs. NAO index				
		Mean	Positive	Positive $p < .05$	Negative	Negative $p < .05$
DAWS	Annual	0.19	83	20.5% (17)	17	5.9% (1)
	Winter	0.55	100	83% (83)	0	0% (0)
	Spring	0.17	90	5.6% (5)	10	10% (1)
	Summer	0.10	71	5.6% (4)	29	10.3% (3)
	Autumn	0.07	63	9.5% (6)	37	10.8% (4)
DPWG	Annual	0.31	83	22.9% (19)	17	0% (0)
	Winter	0.60	100	90% (90)	0	0% (0)
	Spring	0.28	90	17.8% (16)	10	0% (0)
	Summer	0.19	71	12.7% (9)	29	0% (0)
	Autumn	0.1	63	3.2% (2)	37	0% (0)
DAWS freq	Annual	0.20	83	10.8% (9)	17	5.9% (1)
	Winter	0.51	100	79% (79)	0	0% (0)
	Spring	0.25	90	4.4% (4)	10	0% (0)
	Summer	0.11	71	9.9% (7)	29	3.4% (1)
	Autumn	0.11	63	3.2% (2)	3	25% (12)
DPWG freq	Annual	0.09	70	8.6% (6)	30	10% (3)
	Winter	0.42	98	57.1% (56)	2	0% (0)
	Spring	0.12	79	1.3% (1)	21	0% (0)
	Summer	0.06	59	1.7% (3)	41	7.3% (3)
	Autumn	0.03	54	9.3% (5)	46	10.9% (5)

Notes: Relative frequencies are calculated with respect to the total number of stations showing positive or negative correlation.
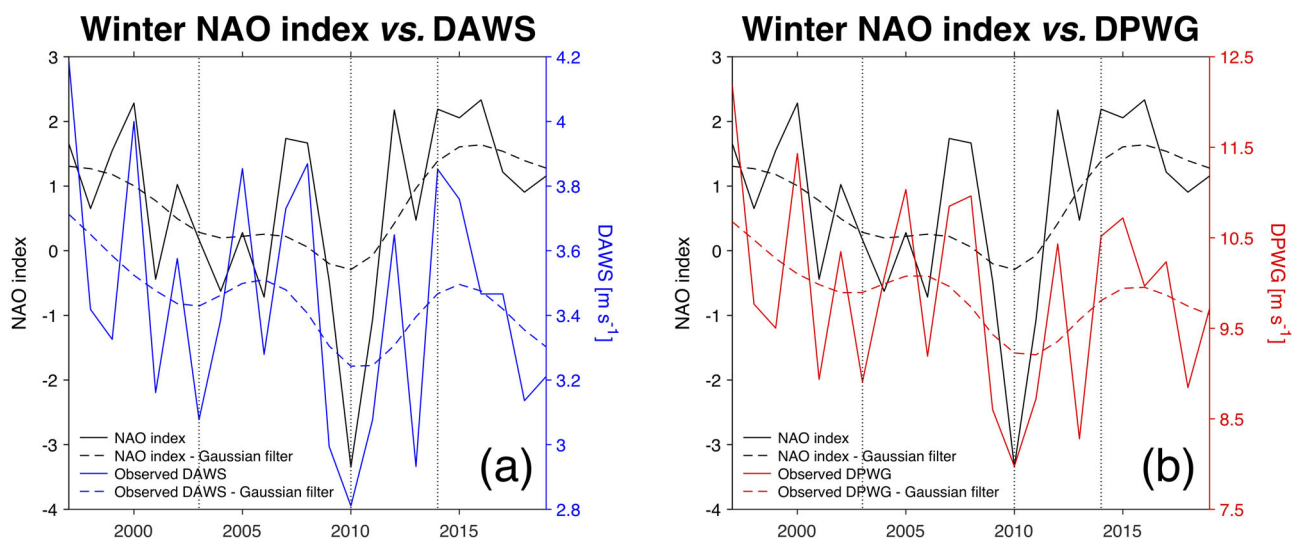

FIGURE 9 Series of winter NAO index versus observed mean (i.e., average over all stations across Sweden) winter DAWS (left) and DPWG (right) for 1997–2019. The low-frequency variability is shown with the dashed lines of the applied Gaussian-weighted average (10-year window) [Colour figure can be viewed at wileyonlinelibrary.com]

TABLE 3 Annual and seasonal relative frequency (%) and number of stations in parentheses showing non-significant and significant ($p < .05$) positive and negative Pearson's correlation coefficient between observed wind series (DAWS, DPWG, DAWS frequency, DPWG frequency) and cyclone statistics (frequency and intensity) for 1997–2019. It is also reported the mean Pearson's correlation coefficient value

		Pearson's correlation coefficient vs. cyclone frequency					Pearson's correlation coefficient vs. cyclone intensity				
		Mean	Positive	Positive $p < .05$	Negative	Negative $p < .05$	Mean	Positive	Positive $p < .05$	Negative	Negative $p < .05$
DAWS	Annual	0.19	89	7.9% (7)	11	0% (0)	−0.33	7	14.3% (1)	93	33.3% (31)
	Winter	0.28	96	13.5% (13)	4	0% (0)	−0.47	1	0% (0)	99	70.7% (70)
	Spring	0.27	91	25.3% (23)	9	0% (0)	−0.39	4	0% (0)	96	56.3% (54)
	Summer	0.18	77	27.3% (21)	23	0% (0)	−0.22	9	0% (0)	91	20.9% (19)
	Autumn	0.08	60	6.7% (4)	39	2.6% (1)	−0.06	36	0% (0)	63	1.6% (1)
DPWG	Annual	0.20	93	8.6% (8)	7	0% (0)	−0.34	2	0% (0)	98	30.6% (30)
	Winter	0.37	99	37.4% (37)	1	0% (0)	−0.52	0	0% (0)	100	80% (80)
	Spring	0.29	97	21.6% (21)	3	0% (0)	−0.33	4	0% (0)	96	22.9% (22)
	Summer	0.10	54	29.6% (16)	46	0% (0)	−0.15	23	0% (0)	77	10.4% (8)
	Autumn	0.21	86	14.0% (12)	13	0% (0)	−0.16	11	0% (0)	88	4.5% (4)
DAWS freq	Annual	0.11	73	8.2% (6)	27	0% (0)	−0.29	9	9% (0)	91	27.5% (25)
	Winter	0.27	95	13.7% (13)	5	0% (0)	−0.48	3	0% (0)	97	72.2% (70)
	Spring	0.22	81	28.6% (24)	19	5.3% (1)	−0.35	7	0% (0)	93	45.2% (42)
	Summer	0.21	80	27.5% (22)	20	0% (0)	−0.23	12	0% (0)	86	26.7% (23)
	Autumn	−0.01	47	6.4% (3)	52	1.9% (1)	−0.06	41	0% (0)	58	8.6% (5)
DPWG freq	Annual	0.15	85	5.8% (5)	15	0% (0)	−0.35	0	0% (0)	100	29% (29)
	Winter	0.45	98	68.4% (67)	2	0% (0)	−0.56	1	0% (0)	99	85.9% (85)
	Spring	0.27	99	20.2% (20)	1	0% (0)	−0.28	9	0% (0)	91	26.7% (27)
	Summer	0.14	71	16.9% (12)	29	0% (0)	−0.10	38	0% (0)	62	19.4% (12)
	Autumn	0.13	67	16.4% (11)	31	0% (0)	−0.21	15	0% (0)	84	20.2% (17)

Notes: Relative frequencies are calculated with respect to the total number of stations showing positive or negative correlation.
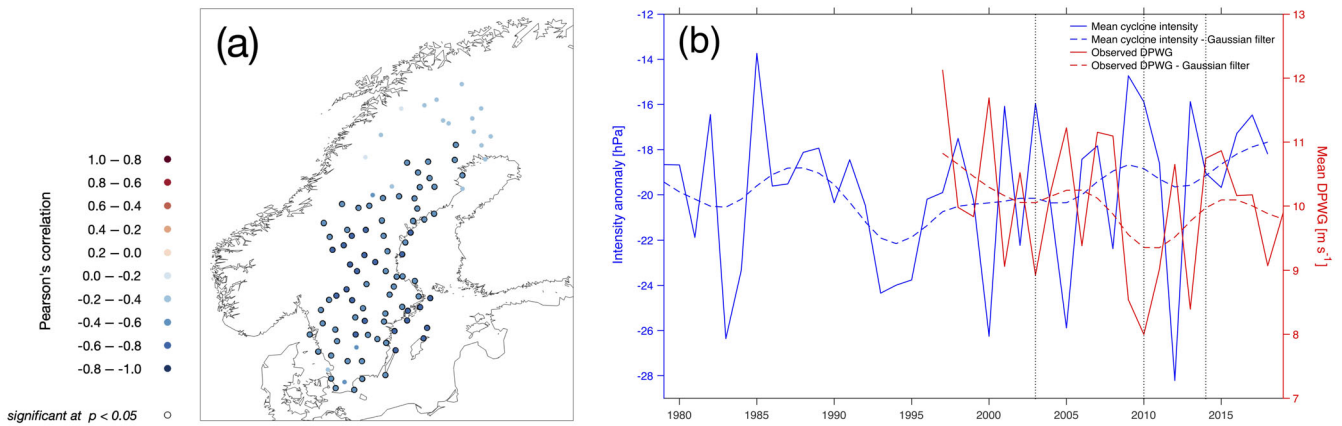
FIGURE 10 Variability of extratropical cyclone intensity. (a) Spatial distribution of Pearson's correlation coefficient between winter cyclone intensity and DPWG for 1997–2018. Circles with a black edge represent stations where correlation is significant at $p < .05$. (b) Series of mean winter cyclone intensity (1979–2038; blue line) and DPWG (1997–2019; red line). The low-frequency variability is shown with the dashed lines of the applied Gaussian-weighted average (10-year window). Mean series are calculated only using stations that show significant (at $p < .05$) negative correlation between winter cyclone intensity and DPWG series [Colour figure can be viewed at wileyonlinelibrary.com]
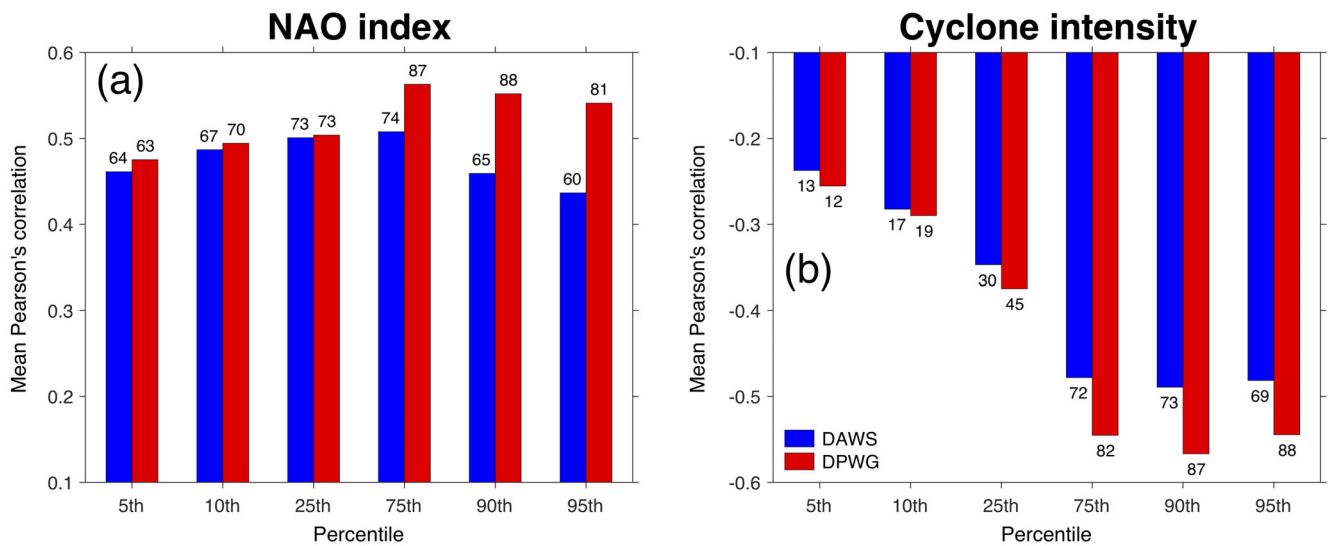

FIGURE 11 Mean winter Pearson's correlation coefficient of NAO index (left) and cyclone intensity (right) with observed DAWS (blue bars) and DPWG (red bars) series during 1997–2019 (1997–2018 when considering cyclone intensity) for various wind intensities (expressed as percentiles). The number over each bar shows the number of stations for the given wind range showing significant correlation at $p < .05$ [Colour figure can be viewed at wileyonlinelibrary.com]

considered MSLP grid points; for intensity, mean correlation is −0.42, which is significant at $p < .05$ for 64% of the grid points.

Figure 11a shows the wintertime correlation of the NAO index to DAWS and DPWG for the range of DAWS and DPWG intensities expressed as percentiles. For NAO, their correlations do not change much for 5th- to 95th-percentile DAWS and DPWG. The same analysis is repeated with the cyclone intensity in Figure 11b. It is found that cyclone intensity shows larger negative correlations for higher DAWS and DPWG intensities, especially

when considering DPWG. These results indicate that while the NAO evenly drives all wind variabilities, extratropical cyclones tend to impact mainly extreme wind values, especially the occurrence of strong wind gusts.

4.4 | Observations versus ERA5 variability

We further compare the observed wind changes with those from ERA5. Figure 12 illustrates both observed and
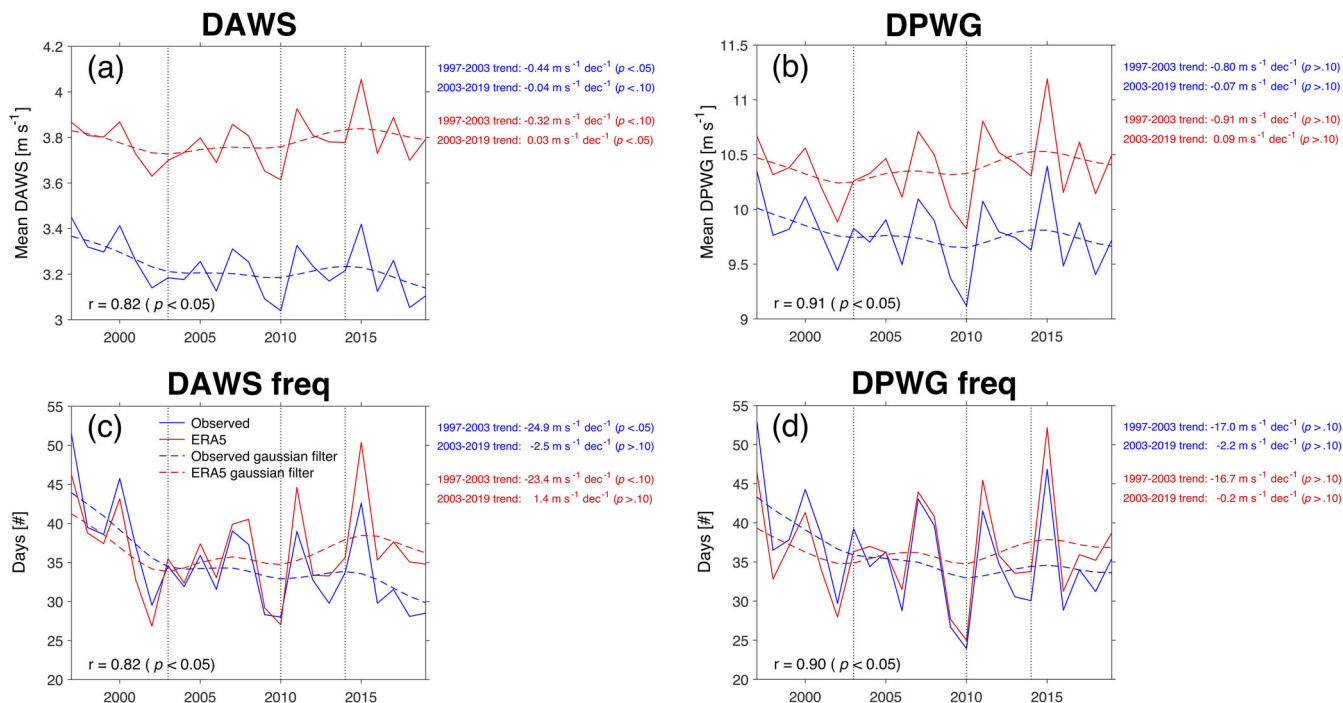
FIGURE 12 Comparison of observed (blue) and ERA5 (red) mean (i.e., average over all stations across Sweden) annual (a) DAWS, (b) DPWG, (c) DAWS frequency and (d) DPWG frequency series from 1997 to 2019. The low-frequency variability is shown by applying a Gaussian-weighted average (10-year window; dashed lines) [Colour figure can be viewed at wileyonlinelibrary.com]
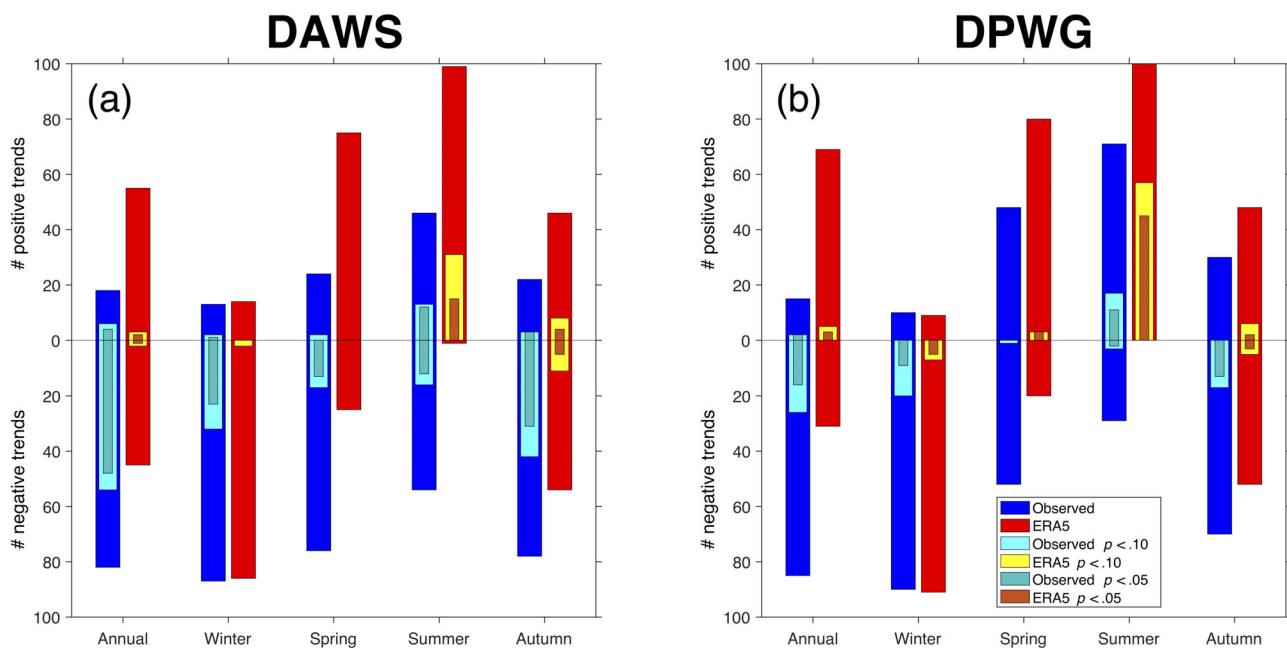

FIGURE 13 Annual and seasonal frequency of positive and negative trends in observed (blue) and ERA5 (red) DAWS (left) and DPWG (right) series across Sweden for 1997–2019. Frequency of significant ($p < .1$ and $p < .05$) trends are also reported [Colour figure can be viewed at wileyonlinelibrary.com]

ERA5 annual wind series for 1997–2019. ERA5 winds follow well the observed variability (correlation higher than 0.8 and significant at $p < .05$), displaying the four phases

in wind changes. This temporal pattern is displayed not only in annual series but also for seasonal series although it is more evident for winter and less noticeable in
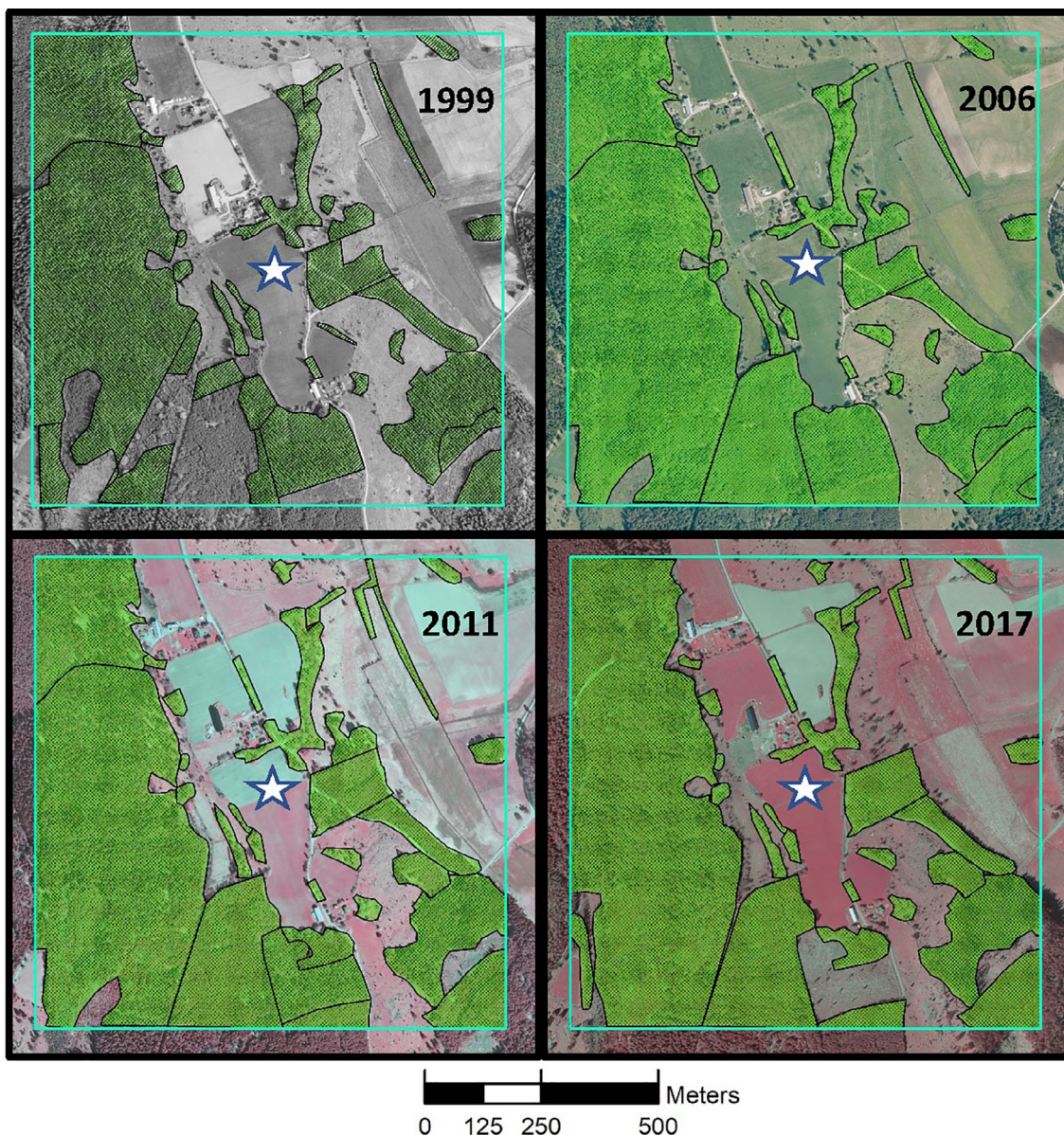
FIGURE 14 Delineation of forest (green hatched areas) around the Malexander A weather station (white star in middle of 1 × 1 km area), shown with background orthophotos from 1999 (panchromatic, 1 m pixel), 2006 (true colour, 0.5 m pixel), 2011 (colour-infrared, 0.5 m pixel) and 2017 (colour-infrared, 0.25 m pixel), GSD-Orthophoto © Lantmäteriet [Colour figure can be viewed at wileyonlinelibrary.com]

summer (not shown here). Even though ERA5 wind series correlate well with the observations, they do not show a general slowdown. This is clearer when looking at Figure 13, where the frequency of positive and negative trends of the observed and ERA5 winds are compared. Both the observations and ERA5 show a higher frequency of negative trends in winter and a greater number of positive trends in summer. However, their trends are overall "more negative" for the observations compared to ERA5, especially when considering only significant trends at $p < .10$ or $p < .05$. This subtle difference could be related to land-use changes which are not considered in reanalysis (Vautard *et al.*, 2010). Changes

in the surface roughness related to the recent increase in vegetation cover for instance are a potential candidate to explain such differences.

4.5 | Impact of surface roughness changes

For all the selected stations, independent of their class (e.g., urban, inland, coastal, etc.), change in forest cover is the main modification that can be detected in the surroundings during the period considered. Figure 14 shows the example of Malexander A measuring station. From

FIGURE 15   Relationship between forest area change (in m^2) between 1998 and 2018 in a 1×1 km area around the weather station, and annual DAWS trend during 1997–2019 for 13 selected weather stations. The black dashed line is the linear fit calculated using all the 13 stations; the red dashed line is the linear fit calculated excluding Skillinge A and Sylarna A stations [Colour figure can be viewed at wileyonlinelibrary.com]
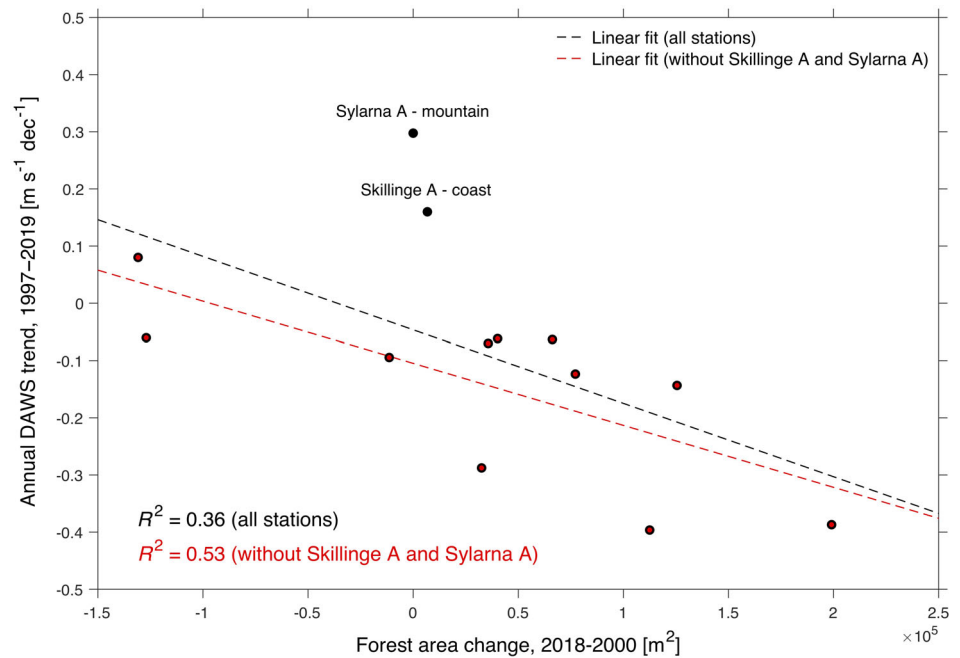
the available orthophotos, it is clear that forest cover in the station surrounding has increased during the last two decades, especially south of its location.

An increase (or decrease) of forest cover and forest growth over years and in proximity to the station's surroundings affects the exposure of the measuring instrument. Consequently, a decrease (or increase) in recorded wind arises from the change of surface roughness in the weather station's proximity. When all 13 sites are used in a linear regression where forest change between 1998 and 2018 is the explanatory variable for annual DAWS trend, the coefficient of determination R^2 is only 0.36 (Figure 15). However, the two outliers are the sites of Skillinge A (coast) and Sylarna A (mountains above tree line) which have little to no forest. These stations had 6,500 and 0 m^2 of forest within the 1×1 km area around the measuring instrument, respectively. Surface roughness change is likely not an influencing factor in these two cases, and their exclusion from the linear regression can be justified. When these two sites are taken out of the analysis, R^2 becomes 0.53 revealing a negative trend relationship between DAWS and forest area (i.e., surface roughness). This result suggests that the increase in forest cover area detected in the proximity of weather stations may partly contribute to the overall slowdown in observed winds, not simulated in v ERA5.

5 | SUMMARY AND DISCUSSION

This study investigated the 1997–2019 variability of homogenized near-surface mean (DAWS) and gust

(DPWG) wind speed across Sweden. Surface mean wind speed changes in Sweden were previously investigated by Minola *et al.* (2016) for 1956–2013. They detected an overall wind decrease over 57 years whose slowdown magnitude is in line with the one reported for nearby countries (e.g., Netherland; Cusack, 2013) or regions of similar latitude range (Canada; Wan *et al.*, 2010). Strong seasonal differences in the changes of wind were also found (e.g., light slowdown/weak increase in winter), revealing the strong influence of large-scale atmospheric circulation (e.g., NAO). In the present study, we look for whether a similar slowdown continues over recent decades (1997–2019) or, as shown by Zeng *et al.* (2019) over Europe, East Asia and North America, where a reversal in the terrestrial stilling can be detected. Our results show that the significant slowdown in DAWS observed since ~1990 (which is dominated by the winter variability) is followed by a non-significant recovery trend from around 2003. Specifically, a stabilization in wind change is observed during 2003–2010; afterwards the winds slightly increase during 2010–2014; and a new slowdown starts since 2014. Given this large low-frequency variability, the detected wind trends are sensitive to the study period considered after 2003 (Troccoli *et al.*, 2012).

The DPWG also underwent four changing phases during 1997–2019, that is, an early slowdown, stabilization, recovery and recent slowdown. The overall agreement in variability between mean and gust wind speeds is consistent with what is observed over the Iberian Peninsula by Azorin-Molina *et al.* (2016), demonstrating that local-to-regional weather systems and teleconnection

patterns with synoptic features are needed to understand wind dynamics across Sweden. Similarly, the occurrence of days with stronger than usual recorded wind shows the same four phases and the same temporal patterns are also seen in the DAWS and DPWG frequencies. A slight difference between DAWS and DPWG variabilities arises only during summer, when synoptic circulation is weaker and local wind systems such as land-sea breezes develop (Gustavsson *et al.*, 1995; Borne *et al.*, 1998).

The great influence of large-scale atmospheric variability on surface wind speed is well known across the high latitudes of Sweden. For example, NAO circulation has a key role in explaining the interannual variability of the surface winds and drives with its positive (and negative) phases the increase (and decrease) of wind during winter (Minola *et al.*, 2016). Indeed, a large pressure difference between the Icelandic low and the Azores high during winter (positive NAO) results in a strong westerly airflow on a more northerly track over Europe (thus across Sweden), forcing low-pressure systems to travel northward, while anticyclonic circulations dominate southern Europe (NOAA, 2012). When both pressure systems are weak (negative NAO), westerlies are also weak and storms track southwards over the Mediterranean Sea, with a resulting increase in storm activity over southern Europe. In fact, we detect that the decadal variabilities of both DAWS and DPWG are significantly correlated with the NAO index especially in winter. This reveals that the four-phase wind changes during 1997–2019 and the recovery of the wind stilling since 2003 are mostly due to the large-scale circulation changes associated with the NAO. This is in line with what was previously observed by Azorin-Molina *et al.* (2018a) over Saudi Arabia or by Kim and Paik (2015) over South Korea. Climate model simulations confirm the impact of large-scale circulation in the wind reversal detected since around 2010, when global surface wind speed trends shifted in their sign due to the negative-to-positive phase changes in the Pacific Decadal Oscillation pattern, which leads to the weakening of the Hadley cell over the Southern Hemisphere and to strengthened westerly winds over the Northern Hemisphere (Deng *et al.*, 2021). This study confirms the large influence of NAO on wind variability; therefore, if we are to make accurate predictions of regional wind change, it is important to understand how NAO will vary in the future. Even though the NAO is a natural mode of atmospheric variability, surface, stratospheric or even anthropogenic processes (e.g., increase in greenhouse gases concentration) may influence its phase and amplitude of variation (Visbeck *et al.*, 2001; Gillet *et al.*, 2003). At present, there is no consensus on the mechanisms that are responsible for the observed multidecadal variations in NAO. This is reflected by climate models which lack ability to simulate NAO variability and leave us uncertain about how NAO will change in the future (Deser *et al.*, 2017). This also implies substantial uncertainty in regional winds across Sweden over the coming decades.

In addition to the NAO teleconnection, the extratropical cyclone activities are also examined to better understand the decadal wind variability across Sweden including a wind stilling-reversal. In fact, extratropical cyclones, growing through baroclinic instability, cause severe weather events including heavy precipitation and strong near-surface winds (Belusic *et al.*, 2019). Previous studies have shown a major cyclone activity area over the North Atlantic Ocean and northwestern Europe (Hoskins and Hodges, 2002), and extratropical cyclones from these regions have a large influence on storminess in Sweden (Belusic *et al.*, 2019). In this study, near-surface wind observations provide evidence of the influence of intensity changes of such low-pressure systems on winter surface winds, especially when it comes to wind gust strength. Their frequency change also affects the occurrence of days of stronger than usual wind gusts. Most importantly, cyclone intensity change agrees well with the wind slow-down observed until 2003 and the absence of a clear trend afterwards indicates that both the large-scale circulation associated with the NAO and extratropical cyclones (which are also partly influenced by the NAO) play a key role in the detected wind stilling-reversal across Sweden. This result further suggests that to estimate future changes in DAWS and DPWG, local cyclone activities need to be better understood in the future. However, as observed here for 1979–2018, there is no clear evidence of multidecadal trends in cyclone frequency or intensity; instead, cyclone location, frequency and intensity showed considerable decadal variability over the past century (Feser *et al.*, 2015; Füssel *et al.*, 2017). There is low confidence in the response of the North Atlantic cyclone statistics to global warming, with model-projections unclear on their possible future evolutions (Christensen *et ali* 2013). For example, as the sign of NAO strongly impacts the frequencies and location of these systems (Keim *et al.*, 2004) and with absence of clear long-term trends in the NAO pattern, it is uncertain how the magnitude of cyclone frequency and intensity will vary under different future scenarios. Therefore, it is still unclear how wind extremes associated with deep low-pressure systems will change in a warmer climate.

Even with large-scale atmospheric circulation dominating wind variability across Sweden (and driving the stilling-recovery), the impact of surface roughness changes is also explored as the possible reason behind the overall slowdown not detected in ERA5. By design, reanalysis products do not include in their hindcasting

the changes in surface roughness (Thorne and Vose, 2010). Increase of surface roughness can be associated with factors such as urbanization, growth of forests, changes in trees and forest distribution or changes in agricultural practices (Yupeng *et al.*, 2019). Previous studies have mainly focused on land-use changes induced by urbanization, with comparison between urban and rural stations (Chen *et al.*, 2020). In this study, we evaluate how wind speed long-term trends can be impacted by surface roughness changes associated with forest cover modifications. Forest cover changes in the proximity of weather stations indeed showed a moderate linear relationship with annual DAWS, indicating that the overall wind slowdown during 1997–2019 is likely partly caused by forest cover increase. Vautard *et al.* (2010) used Normalized Difference Vegetation Index (NDVI) from satellite images, indicating that increased NDVI had an impact on wind speed trends. We used orthophotos rather than NDVI, given the orthophoto's advantages of high spatial resolution (0.25–1 m grid cells) at good temporal resolution, as well as better differentiation between seasonal agricultural change and forest growth, which can be difficult to discern based only on NDVI. Vautard *et al.* (2010) also state that a quantitative relationship between NDVI and land roughness is hard to establish. As LiDAR data become increasingly available, forest height and density metrics can be useful for future analysis of surface roughness change and status around weather stations.

It is further found that the highest percentiles in both the DAWS and DPWG distributions underwent the greatest changes and largest fluctuations compared to the lowest ones: that is, strong winds, rather than weak winds, drive most of the changes in wind variability across Sweden. This inhomogeneity, which was also observed by Zhang and Wang (2020) across China, is simulated by climate models under future global climate scenarios (Jung and Schindler, 2019). Such changes in the wind distribution can have a huge impact on wind power production as the wind resource is largely guided by the upper percentiles of the wind speed distribution (Pryor and Berthelmie, 2010). This is amplified by the nonlinear relationship between wind speed and power production from a wind turbine (i.e., the wind turbine power curve). In a similar way, also changes in gusts are stronger than the ones observed for mean wind speed. When mean wind speed increases, the atmosphere becomes even more turbulent. Such difference in gust and mean wind speed changes can strongly affect wind turbine energy production as the ambient turbulent intensity impact is different at different wind speeds (Lubitz, 2014): at low wind speeds, an increase in gust turbulence increases turbine energy production, while at wind speeds near the turbine furling speed, strong turbulence results in decreased energy production.

6 | CONCLUSIONS

To summarize, the major findings of this study are the following:

- A break in the stilling is identified in the recent past for both near-surface mean and gust wind speed across Sweden: the significant ($p < .05$) slowdown detected until 2003 at most of the weather stations is followed by lack of a clear trend afterwards.
- The observed stilling-reversal is possibly linked to the recent changes in large-scale atmospheric circulation, such as NAO teleconnection pattern and cyclone activity.
- The changes in strong winds are much larger than in weak winds. In a similar way, increases in wind gusts are larger compared to changes in mean wind speed.
- Even with atmospheric circulation driving most of the wind variability across Sweden, forest cover increases detected in the wind instrument surroundings during the last two decades have also likely contributed to decreasing wind trends, not found in the ERA5 reanalysis.

To conclude, changes in terrestrial near-surface winds can be induced by a combination of different causes, from anthropogenic activities to natural climate changes. In this study, atmospheric circulation associated with the NAO and cyclone activity changes are confirmed to be the driving factor behind the stilling and the recent recovery of surface winds across Sweden, in line with what is observed for near-surface winds across different mid-latitude regions (Kim and Paik, 2015; Azorin-Molina *et al.*, 2018a; Zeng *et al.*, 2019). The observed reduction of surface wind speed is also partly attributed to land use and cover change, as similarly shown by Vautard *et al.* (2010) and Wever (2012). But decadal wind variability in this study is only qualitatively related to both atmospheric circulation and surface roughness changes. Future work should quantify and distinguish the sources of these changes in the driving forces (Wu *et al.*, 2018).

AUTHOR CONTRIBUTIONS

Lorenzo Minola: Conceptualization; data curation; formal analysis; investigation; methodology; project administration; visualization; writing-original draft. **Heather Reese:** Formal analysis; investigation; methodology; visualization; writing-review & editing. **Hui-Wen Lai:** Formal analysis; investigation; methodology; visualization; writing-review & editing. **Cesar Azorin-Molina:** Supervision; writing-review & editing. **José Guijarro:** Methodology; writing-review & editing. **Seok-Woo Son:** Methodology; writing-review & editing. **Deliang Chen:** Conceptualization; funding acquisition; supervision; writing-review & editing.

ORCID

Hui-Wen Lai https://orcid.org/0000-0003-3813-0276
Cesar Azorin-Molina https://orcid.org/0000-0001-5913-7026
Deliang Chen https://orcid.org/0000-0003-0288-5618

REFERENCES

Abhishek, A., Lee, J.-Y., Keener, T.C. and Yang, Y.J. (2012) Long-term wind speed variations for three midwestern U.S. cities. *Journal of the Air & Waste Management Association*, 60(9), 1057–1064. https://doi.org/10.3155/1047-3289.60.9.1057.

Achberger, C., Chen, D. and Alexandersson, H. (2006) The surface winds of Sweden during 1999–2000. *International Journal of Climatology*, 26(2), 159–178. https://doi.org/10.1002/joc.1254.

Aguilar, E., Auer, I., Brunet, M., Peterson, T.C. and Wieringa, J. (2003) *Guidelines on Climate Metadata and Homogenization*. Geneva: WMO, pp. 52. Available at:. https://library.wmo.int/doc_num.php?explnum_id=9252 .

Azorin-Molina, C., Vicente-Serrano, S.M., McVicar, T.R., Jerez, S., Sanchez-Lorenzo, A., López-Moreno, J.-I., Revuelto, J., Trigo, R.M., Lopez-Bustins, J.A. and Espíritp-Santo, F. (2014) Homogenization and assessment of observed near-surface wind speed trends over Spain and Portugal, 1961–2011. *Journal of Climate*, 27(10), 3692–3712. https://doi.org/10.1175/JCLI-D-13-00652.1.

Azorin-Molina, C., Guijarro, J.A., McVicar, T.R., Vicente-Serrano, S.M., Chen, D., Jerez, S. and Espírito-Santo, F. (2016) Trends of daily peak wind gusts in Spain and Portugal, 1961–2014. *Journal of Geophysical Research—Atmospheres*, 121, 1059–1078. https://doi.org/10.1002/2015JD024485.

Azorin-Molina, C., Rehman, S., Guijarro, J.A., McVicar, T.R., Minola, L., Chen, D. and Vicente-Serrano, S.M. (2018a) Recent trends in wind speed across Saudi Arabia, 1978–2013: a break in the stilling. *International Journal of Climatology*, 38(S1), e966–e984. https://doi.org/10.1002/joc.5423.

Azorin-Molina, C., Asin, J., McVicar, T.R., Minola, L., Lopez-Moreno, J.I., Vicente-Serrano, S.M. and Chen, D. (2018b) Evaluating anemometer drift: a statistical approach to correct biases in wind speed measurement. *Atmospheric Research*, 203, 175–188. https://doi.org/10.1016/j.atmosres.2017.12.010.

Azorin-Molina, C., McVicar, T. R., Guijarro, J. A., Trewin, B., Frost, A. J., Zhang, G., Minola, L., Son, S.-W., Deng, K. and Chen, D. (2021) A decline of observed daily peak wind gusts with distinct seasonality in Australia, 1941–2016. *Journal of Climate*, 34(8), 3103–3127. https://doi.org/10.1175/JCLI-D-20-0590.1.

Baker, A.J., Schiemann, R., Hodges, K.I., Demory, M.-E., Mizielinski, M.S., Roberts, M.J., Shaffrey, L.C., Strachan, J. and Vidale, P.L. (2019) Enhanced climate change response of wintertime North-Atlantic circulation, cyclone activity, and precipitation in a 25-km-resolution global atmospheric model. *Journal of Climate*, 32(22), 7763–7781. https://doi.org/10.1175/JCLI-D-19-0054.1.

Beljaars, A.C.M. (1987) *The Measurement of Gustiness at Routine Wind Stations—A Review*. Geneva: WMO, pp. 52. Available at:. https://library.wmo.int/doc_num.php?explnum_id=7372 .

Belusic, D., Berg, P., Bozhinova, D., Bärring, L., Döscher, R., Eronn, A., Kjellström, E., Klehmet, K., Martins, H., Nilsson, C., Olsson, J., Photiadou, C., Segersson, D. and Strandberg, G. (2019) *Climate Extremes for Sweden*. Norrköping: SMHI, pp. 14–19. Available at:. http://smhi.diva-portal.org/smash/get/diva2:1368107/FULLTEXT01.pdf .

Borne, K., Chen, D. and Nunez, M. (1998) A method for finding sea breeze days under stable synoptic conditions and its application to the Swedish west coast. *International Journal of Climatology*, 18(8), 901–914. https://doi.org/10.1002/(SICI)1097-0088(19980630)18:8<901::AID-JOC295>3.0.CO;2-F.

Buchan, J., Hirschi, J.J.-M., Blaker, A.T. and Sinha, B. (2014) North Atlantic SST anomalies and the cold north European weather events of winter 2009/10 and December 2010. *Monthly Weather Review*, 142(2), 922–932. https://doi.org/10.1175/MWR-D-13-00104.1.

Chen, D. and Hellström, C. (1999) The influence of the North Atlantic oscillation on the regional temperature variability in Sweden: spatial and temporal variations. *Tellus*, 51A, 505–516. https://doi.org/10.3402/tellusa.v51i4.14086.

Chen, X., Jeong, S., Park, H., Kim, J. and Park, C.-R. (2020) Urbanization has stronger impacts than regional climate change on wind stilling: a lesson from South Korea. *Environmental Research Letters*, 15, 054016. https://doi.org/10.1088/1748-9326/ab7e51.

Christensen, J.H., Krishna Kumar, K., Aldrian, E., An, S.-I., Cavalcanti, I.F.A., de Castro, M., Dong, W., Goswami, P., Hall, A., Kanyanga, J.K., Kitoh, A., Kossin, J., Lau, N.-C., Renwick, J., Stephenson, D.B., Xie, S.-P. and Zhou, T. (2013) Climate phenomena and their relevance for future regional climate change. In: Stocker, T.F., Qin, D., Plattner, G.-K., Tignor, M., Allen, S.K., Boschung, J., Nauels, A., Xia, Y., Bex, V. and Midgley, P.M. (Eds.) *Climate Change 2013: The*

Physical Science Basis. Cambridge: Cambridge University Press, pp. 1217–1308.

Cusack, S. (2013) A 101 year record of windstorms in the Netherlands. *Climatic Change*, 116, 693–704. https://doi.org/10.1007/s10584-012-0527-0.

Dee, D.P., Uppala, S.M., Simmons, A.J., Berrisford, P., Poli, P., Kobayashi, S., Andrae, U., Balmaseda, M.A., Balsamo, G., Bauer, P., Bechtold, P., Beljaars, A.C.M., van de Berg, L., Bidlot, J., Bormann, N., Delsol, C., Dragani, R., Duentes, M., Geer, A.J., Haimberger, L., Healy, S.B., Hersbach, H., Hólm, E.V., Isaksen, L., Kållberg, P., Köhler, M., Matricardi, M., McNally, A.P., Monge-Sanz, B.M., Morcrette, J.-J., Park, B.-K., Peubey, C., de Rosnay, P., Tavolato, C., Thépaut, J.-N. and Vitart, F. (2011) The ERA-Interim reanalysis: configuration and performance of the data assimilation system. *Quarterly Journal of Royal Meteorological Society*, 137(656), 553–597. https://doi.org/10.1002/qj.828.

Deng, K., Azorin-Molina, C., Minola, L., Zhang, G. and Chen, D. (2021) Global near-surface wind speed changes over the last decades revealed by reanalyses and CMIP6 model simulations. *Journal of Climate*, 34(6), 2219–2234. https://doi.org/10.1175/JCLI-D-20-0310.1.

Deser, C., Hurrell, J.W. and Phillips, A.S. (2017) The role of the North Atlantic oscillation in European climate projections. *Climate Dynamics*, 49, 3141–3157. https://doi.org/10.1007/s00382-016-3502-z.

Feser, F., Barcikowska, M., Krueger, O., Schenk, F., Weisse, R. and Xia, L. (2015) Storminess over the North Atlantic and north-western Europe—a review. *Quarterly Journal of the Royal Meteorological Society*, 141(687), 350–382. https://doi.org/10.1002/qj.2364.

Füssel, H.-M., Jol, A., Marx, A. and Hildén, M. (2017) *Climate Change, Impacts and Vulnerability in Europe 2016—An Indicator-Based Report*. Copenhagen: European Environmental Agency, p. 419. Available at:. https://climate-adapt.eea.europa.eu/metadata/publications/climate-change-impacts-and-vulnerability-in-europe-2016/climate-change-impacts-and-vulnerabilities-2016-thal17001enn.pdf .

Gibbons, J.D. and Chakraborti, S. (2011) Nonparametric statistical inference. In: Lovric, M. (Ed.) *International Encyclopedia of Statistical Science*, 1st edition. Berlin: Springer, pp. 937–1013.

Gilbert, R.O. (1987) *Statistical Method for Environmental Pollution Monitoring*. New York: Van Nostrand Reinhold Co., p. 320.

Gillet, N.P., Graf, H.F. and Osborn, T.J. (2003) Climate change and the North Atlantic oscillation. In: Hurrell, J.W. (Ed.) *The North Atlantic Oscillation: Climatic Significance and Environmental Impact*, Geophysical Monograph Series, 134. Washington, DC: AGU, pp. 193–209. https://doi.org/10.1029/134gm09.

Grise, K.M., Son, S.-W. and Gyakum, J.R. (2013) Intraseasonal and interannual variability in North American storm tracks and its relationship to equatorial Pacific variability. *Monthly Weather Review*, 141(10), 3610–3625. https://doi.org/10.1175/MWR-D-12-00322.1.

Grundström, M., Linderholm, H.W., Klingberg, J. and Pleijel, H. (2011) Urban NO_2 and NO pollution in relation to the North Atlantic oscillation NAO. *Atmospheric Environment*, 45(4), 883–888. https://doi.org/10.1016/j.atmosenv.2010.11.023.

Grundström, M., Hak, C., Chen, D., Hallquist, M. and Pleijel, H. (2015) Variation and co-variation of PM_{10}, particle number concentration, NO_X and NO_2 in the urban air—relationships with wind speed, vertical temperature gradient and weather type.

Atmospheric Environment, 120, 317–327. https://doi.org/10.1016/j.atmosenv.2015.08.057.

Guijarro, J.A. (2017) Daily series homogenization and gridding with Climatol v.3. In: *Ninth Seminar for Homogenization and Quality Control in Climatological Databases and Fourth Conference on Spatial Interpolation Techniques in Climatology and Meteorology*. Budapest: WMO, pp. 175–180. Available at:. https://library.wmo.int/doc_num.php?explnum_id=5680 .

Gustavsson, T., Lindqvist, S., Borne, K. and Bogren, J. (1995) A study of land and sea breezes in an archipelago on the west coast of Sweden. *International Journal of Climatology*, 15(7), 785–800. https://doi.org/10.1002/joc.3370150706.

Haanpää, S., Lehtonen, S., Peltonen, L. and Talockaite, E. (2007) *Impacts of Winter Storm Gudrun of 7th–9th January 2005 and Measures Taken in Baltic Sea Region*. Espoo: ASTRA Project, p. 43. Available at:. https://discomap.eea.europa.eu/map/Data/Milieu/OURCOAST_110_Baltic/OURCOAST_110_Baltic_Doc1_ImpactGudrunStorm.pdf .

Hamed, K.H. and Ramachandra Rao, A. (1998) A modified Mann-Kendall trend test for autocorrelated data. *Journal of Hydrology*, 204(1–4), 182–196. https://doi.org/10.1016/S0022-1694(97)00125-X.

Hannon Bradshaw, L. (2017) Sweden, forests and wind storms: developing a model to predict storm damage to forests in Kronoberg County. Master. Lund University.

Hersbach, H., de Rosnay, P., Bell, B., Schepers, D., Simmons, A., Soci, C., Abdalla, S., Alonso Balmaseda, M., Balsamo, G., Bechtold, P., Berrisford, P., Bidlot, J., de Boisséson, E., Bonavita, M., Browne, P., Buizza, R., Dahgren, P., Dee, D., Dragani, R., Diamantakis, M., Flemming, J., Forbes, R., Geer, A., Haiden, T., Hólm, E., Haimberger, L., Hogan, R., Horányi, A., Janisková, M., Laloyaux, P., Lopez, P., Muñoz-Sabater, J., Peubey, C., Radu, R., Richardson, D., Thépaut, J.-N., Vitart, F., Yang, X., Zsótér, E. and Zuo, H. (2018) *Operational Global Reanalysis: Progress, Future Directions and Synergies with NWP*. ERA Report Series 27. Reading, MA: ECMWF, p. 63. Available at:. https://www.ecmwf.int/en/elibrary/18765-operational-global-reanalysis-progress-future-directions-and-synergies-nwp .

Hewson, T.D. and Titley, H.A. (2010) Objective identification, typing and tracking of the complete life-cycles of cyclonic features at high spatial resolution. *Meteorological Applications*, 17(3), 355–381. https://doi.org/10.1002/met.204.

Hodges, K.I. (1994) A general method for tracking analysis and its application to meteorological data. *Monthly Weather Review*, 122(11), 2573–2586. https://doi.org/10.1175/1520-0493(1994)122<2573:AGMFTA>2.0.CO;2.

Hodges, K.I. (1995) Feature tracking on the unit sphere. *Monthly Weather Review*, 123(12), 3458–3465. https://doi.org/10.1175/1520-0493(1995)123<3458:FTOTUS>2.0.CO;2.

Hodges, K.I. (1996) Spherical nonparametric estimators applied to the UGAMP model integration for AMIP. *Monthly Weather Review*, 124(12), 2914–2932. https://doi.org/10.1175/1520-0493(1996)124<2914:SNEATT>2.0.CO;2.

Hodges, K.I., Hoskins, B.J., Boyle, J. and Thorncroft, C. (2003) A comparison of recent reanalysis datasets using objective feature tracking: storm tracks and tropical easterly waves. *Monthly Weather Review*, 131(9), 2012–2037. https://doi.org/10.1175/1520-0493(2003)131<2012:ACORRD>2.0.CO;2.

Hoskins, B.J. and Hodges, K.I. (2002) New perspectives on the northern hemisphere winter storm tracks. *Journal of the Atmospheric Sciences*, 59(6), 1041–1061. https://doi.org/10.1175/1520-0469(2002)059<1041:NPOTNH>2.0.CO;2.

Hurrell, J.W. (1995) Decadal trends in the North Atlantic oscillation: regional temperatures and precipitation. *Science*, 269 (5224), 676–679. https://doi.org/10.1126/science.269.5224.676.

Hurrell, J.W. and van Loon, H. (1997) Decadal variations in climate associated with the North Atlantic oscillation. *Climatic Change*, 36, 301–326. https://doi.org/10.1023/A:1005314315270.

Jeong, J.-H., Walther, A., Nikulin, G., Chen, D. and Jones, C. (2011) Diurnal cycle of precipitation amount and frequency in Sweden: observation versus model simulation. *Tellus A*, 63(4), 664–674. https://doi.org/10.1111/j.1600-0870.2011.00517.x.

Jones, P.D., Jonsson, T. and Wheeler, D. (1997) Extension of the North Atlantic oscillation using early instrumental pressure observations from Gibraltar and south-West Iceland. *International Journal of Climatology*, 17(13), 1433–1450. https://doi.org/10.1002/(SICI)1097-0088(19971115)17:13<1433::AID-JOC203>3.0.CO;2-P.

Jung, C. and Schindler, D. (2019) Changing wind speed distributions under future global climate. *Energy Conversion and Management*, 198, 111841. https://doi.org/10.1016/j.enconman.2019.111841.

Keim, B.D., Muller, R.A. and Stone, G.W. (2004) Spatial and temporal variability of coastal storms in the North Atlantic Basin. *Marine Geology*, 210, 7–15. https://doi.org/10.1016/j.margeo.2003.12.006.

Kim, J. and Paik, K. (2015) Recent recovery of surface wind speed after decadal decrease: a focus on South Korea. *Climate Dynamics*, 45, 1699–1712. https://doi.org/10.1007/s00382-015-2546-9.

Kwon, D.K. and Kareem, A. (2014) Revisiting gust averaging time and gust effect factor in ASCE 7. *Journal of Structural Engineering*, 140(11), 06014004. https://doi.org/10.1061/(ASCE)ST.1943-541X.0001102.

Lee, J., Son, S.-W., Cho, H.-Ö., Kim, J., Cha, D.-H., Gyakum, J.R. and Chen, D. (2020) Extratropical cyclones over East Asia: climatology, seasonal cycle, and long-term trend. *Climate Dynamics*, 54, 1131–1144. https://doi.org/10.1007/s00382-019-05048-w.

Lin, C., Yang, K., Qin, J. and Fu, R. (2013) Observed coherent trends of surface and upper-air wind speed over China since 1960. *Journal of Climate*, 26(9), 1891–2903. https://doi.org/10.1175/JCLI-D-12-00091.1.

Linderholm, H.W., Ou, T., Jeong, J.-H., Folland, C.K., Gong, D., Liu, H., Liu, Y. and Chen, D. (2011) Interannual teleconnections between the summer North Atlantic oscillation and the east Asian summer monsoon. *Journal of Geophysical Research—Atmospheres*, 116, D13107. https://doi.org/10.1029/2010JD015235.

Lubitz, W.D. (2014) Impact of ambient turbulence on performance of a small wind turbine. *Renewable Energy*, 61, 69–73. https://doi.org/10.1016/j.renene.2012.08.015.

McVicar, T.R., Roderick, M.L., Donohue, R.J., Li Tao, L., Van Niel, T.G., Thomas, A., Grieser, J., Jhajharia, D., Himri, Y., Mahowald, N.M., Mescherskaya, A.V., Kruger, A.C., Rehman, S. and Dinpasoh, Y. (2012) Global review and synthesis of trends in observed terrestrial near-surface wind speeds: implications for evaporation. *Journal of Hydrology*, 416–417, 182–205. https://doi.org/10.1016/j.jhydrol.2011.10.024.

Miao, H., Dong, D., Huang, G., Hu, K., Tian, Q. and Gong, Y. (2020) Evaluation of northern hemisphere surface wind speed and wind power density in multiple reanalysis datasets. *Energy*, 200, 117382. https://doi.org/10.1016/j.energy.2020.117382.

Minola, L., Azorin-Molina, C. and Chen, D. (2016) Homogenization and assessment of observed near-surface wind speed trends across Sweden, 1956–2013. *Journal of Climate*, 29(20), 7397–7415. https://doi.org/10.1175/JCLI-D-15-0636.1.

Minola, L., Zhang, F., Azorin-Molina, C., Safaei Pirroz, A.A., Flay, R.G.J., Hersbach, H. and Chen, D. (2020) Near-surface mean and gust wind speeds in ERA5 across Sweden: towards an improved gust parametrization. *Climate Dynamics*, 55, 887–907. https://doi.org/10.1007/s00382-020-05302-6.

Minola, L., Azorin-Molina, C., Guijarro, J.A., Zhang, G., Son, S.-W. and Chen, D. (2021) Climatology of near-surface daily peak wind gusts across Scandinavia: observations and model simulations. *Journal of Geophysical Research – Atmospheres*, 126(7), e2020JD033534. https://doi.org/10.1029/2020JD033534.

National Oceanic and Atmospheric Administration (NOAA) (2012) *North Atlantic Oscillation (NAO)*. College Park: Climate Prediction Center. Available at: https://www.cpc.ncep.noaa.gov/data/teledoc/nao.shtml []

Neu, U., Akperov, M.G., Bellenbaum, N., Benestad, R., Blender, R., Caballero, R., Cocozza, A., Dacre, H.F., Feng, Y., Fraedrich, K., Grieger, J., Gulev, S., Hanley, J., Hewson, T., Inatsu, M., Keay, K., Kew, S.F., Kindem, I., Leckebusch, G.C., Liberato, M.L.R., Lionello, P., Mokhov, I.I., Pinto, J.G., Raible, C.C., Reale, M., Rudeva, I., Schuster, M., Simmonds, I., Sinclair, M., Sprenger, M., Tilinina, N.D., Trigo, I.F., Ulbrich, S., Ulbrich, U., Wang, X.L. and Wernli, H. (2013) IMILAST: a community effort to intercompare extratropical cyclone detection and tracking algorithms. *Bulletin of the American Meteorological Society*, 94(4), 529–547. https://doi.org/10.1175/BAMS-D-11-00154.1.

Pryor, S.C., Barthelmie, R.J. and Schoof, J.T. (2005) Inter-annual variability of wind indices across Europe. *Wind Energy*, 9(1–2), 27–38. https://doi.org/10.1002/we.178.

Pryor, S.C. and Berthelmie, R.J. (2010) Climate change impacts on wind energy: a review. *Renewable and Sustainable Energy Reviews*, 14(1), 430–437. https://doi.org/10.1016/j.rser.2009.07.028.

Punkka, A.-J. and Bister, M. (2015) Mesoscale convective systems and their synoptic-scale environment in Finland. *Weather and Forecasting*, 30(1), 182–196. https://doi.org/10.1175/WAF-D-13-00146.1.

Ramon, J., Lledó, L., Torralba, V., Soret, A. and Doblas-Reyes, F.J. (2019) What global reanalysis best represents near-surface winds? *Quarterly Journal of the Royal Meteorological Society*, 145, 3236–3251. https://doi.org/10.1002/qj.3616.

Rayner, D.P. (2007) Wind run changes: the dominant factor affecting pan evaporation trends in Australia. *Journal of Climate*, 20 (14), 3379–3394. https://doi.org/10.1175/JCLI4181.1.

Roderick, M.L., Rotstayn, L.D., Farquhar, G.D. and Hobbins, M.T. (2007) On the attribution of changing pan evaporation. *Geophysical Research Letters*, 34(17), L17403. https://doi.org/10.1029/2007GL031166.

Swedish Commission on Climate and Vulnerability. (2007) *Sweden Facing Climate Change—Threats and Opportunities*. Stockholm: SOU, pp. 92–96. Available at:. https://www.government.se/

49b75f/contentassets/5f22ceb87f0d433898c918c2260e51aa/sweden-facing-climate-change-sou-200760 .

Suomi, I., Gryning, S.-E., Floors, R., Vihma, T. and Fortelius, C. (2014) On the vertical structure of wind gusts. *Quarterly Journal of the Royal Meteorological Society*, 141(690), 1658–1670. https://doi.org/10.1002/qj.2468.

Thorne, P.W. and Vose, R.S. (2010) Reanalyses suitable for characterizing long-term trends. *Bulletin of the American Meteorological Society*, 91(3), 353–362. https://doi.org/10.1175/2009BAMS2858.1.

Tokinaga, H. and Xie, S.-P. (2011) Wave- and anemometer-based sea surface wind (WASWind) for climate change analysis. *Journal of Climate*, 24(1), 267–285. https://doi.org/10.1175/2010JCLI3789.1.

Troccoli, A., Muller, K., Coppin, P., Davy, R., Russell, C. and Hirsch, A.L. (2012) Long-term wind speed trends over Australia. *Journal of Climate*, 25(1), 170–183. https://doi.org/10.1175/2011JCLI4198.1.

Vautard, R., Cattiaux, J., Yiou, P., Thépaut, J.-N. and Ciais, P. (2010) Northern hemisphere atmospheric stilling partly attributed to an increase in surface roughness. *Nature Geoscience*, 3, 756–761. https://doi.org/10.1038/NGEO979.

Visbeck, M.H., Hurrell, J.W., Polvani, L. and Cullen, H.M. (2001) The North Atlantic oscillation: past, present, and future. *Proceeding of the national Academy of Sciences of the United States of America*, 98(23), 12876–12877. https://doi.org/10.1073/pnas.231391598.

Vose, R.S., Applequist, S., Bourassa, M.A., Pryor, S.C., Barthelmie, R.J., Blanton, B., Bromirski, P.D., Brooks, H.E., DeGaetano, A.T., Dole, R.M., Easteriling, D.R., Jensen, R.E., Karl, T.R., Katz, R.W., Klink, K., Kruk, M.C., Kunkel, K.E., MacCracken, M.C., Peterson, T.C., Shein, K., Thomas, B.R., Walsh, J.E., Wang, X.L., Wehner, M.F., Wuebbles, D.J. and Young, R.S. (2014) Monitoring and understanding changes in extremes: extratropical storms, winds, and waves. *Bulletin of American Meteorological Society*, 95(3), 377–386. https://doi.org/10.1175/BAMS-D-12-00162.1.

Wallace, J.M. and Gutzler, D.S. (1981) Teleconnections in the geopotential height field during the northern hemisphere winter. *Monthly Weather Review*, 109(4), 784–812. https://doi.org/10.1175/1520-0493(1981)109<0784:TITGHF>2.0.CO;2.

Wan, H., Wang, X.L. and Swail, V.R. (2010) Homogenization and trend analysis of Canadian near-surface wind speeds. *Journal of Climate*, 23(5), 1209–1225. https://doi.org/10.1175/2009JCLI3200.1.

Weatherhead, E.C., Reinsel, G.C., Tiao, G.C., Meng, X.-L., Choi, D., Cheang, W.-K., Keller, T., DeLuisi, J., Wuebbles, D.J., Kerr, J.B., Miller, A.J., Oltmans, S.J. and Fredrick, J.E. (1998) Factors affecting the detection of trends: statistical considerations and applications to environmental data. *Journal of Geophysical Research—Atmospheres*, 103(D14), 17149–17161. https://doi.org/10.1029/98JD00995.

Wern, L. and Bärring, L. (2009) *Sveriges vindklimat 1901–2008: Analys av trend i geostrofik vind*. Norrköping: SMHI, p. 72. Available at:. http://www.smhi.se/polopoly_fs/1.7843!/meteorologi_138.pdf .

Wever, N. (2012) Quantifying trends in surface roughness and the effect on surface wind speed observations. *Journal of Geophysical Research—Atmospheres*, 117, D11104. https://doi.org/10.1029/2011JD017118.

Wohland, J., Omrani, N.-E., Witthaut, D. and Keenlyside, N.S. (2019) Inconsistent wind speed trends in current twentieth century reanalyses. *Journal of Geophysical Research—Atmospheres*, 124(4), 1931–1940. https://doi.org/10.1029/2018JD030083.

World Meteorological Organization (WMO). (2014) *Guide to Meteorological Instruments and Methods of Observations*. Geneva: WMO, p. 72. Available at. https://www.weather.gov/media/epz/mesonet/CWOP-WMO8.pdf .

Wu, J., Zha, J., Zhao, D. and Yang, Q. (2018) Changes in terrestrial near-surface wind speed and their possible causes: an overview. *Climate Dynamics*, 51, 2039–2078. https://doi.org/10.1007/s00382-017-3997-y.

Young, I.R. and Ribal, A. (2019) Multiplatform evaluation of global trends in wind speed and wave height. *Science*, 364(6440), 548–552. https://doi.org/10.1126/science.aav9527.

Yu, J., Zhou, T., Jiang, Z. and Zou, L. (2019) Evaluation of near-surface wind speed changes during 1979 to 2011 over China based on five reanalysis datasets. *Atmosphere*, 10(12), 804. https://doi.org/10.3390/atmos10120804.

Yupeng, L., Yaning, C. and Zhi, L. (2019) Effects of land use and cover change on surface wind speed in China. *Journal of Arid Land*, 11, 345–356. https://doi.org/10.1007/s40333-019-0095-5.

Zeng, Z., Pia, S., Li, L.Z.X., Ciais, P., Li, Y., Cai, X., Yang, L., Liu, M. and Wood, E.F. (2018) Global terrestrail stilling: does Earth's greening play a role? *Environmental Research Letters*, 13, 124013. https://doi.org/10.1088/1748-9326/aaea84.

Zeng, Z., Ziegler, A.D., Searchinger, T., Yang, L., Chen, A., Ju, K., Piao, S., Li, L.Z.X., Ciais, P., Chen, D., Liu, J., Azorin-Molina, C., Chappell, A., Medvigy, D. and Wood, E.F. (2019) A reversal in global terrestrial stilling and its implications for wind energy production. *Nature Climate Change*, 9, 979–985. https://doi.org/10.1038/s41558-019-0622-6.

Zhang, Z., Wang, K., Chen, D., Li, J. and Diskinson, R. (2019) Increase in surface friction dominated the observed surface wind speed decline during 1973–2014 in the northern hemisphere lands. *Journal of Climate*, 32 (21), 7421–7435. https:/7doi.org/https://doi.org/10.1175/JCLI-D-18-0691.1

Zhang, G., Azorin-Molina, C., Chen, D., Guijarro, J.A., Kong, F., Minola, L., McVicar, T.R., Son, S.-W. and Shi, P. (2020) Variability of daily maximum wind speed across China, 1975–2016: an examination of likely causes. *Journal of Climate*, 33(7), 2793–2816. https://doi.org/10.1175/JCLI-D-19-0603.1.

Zhang, Z. and Wang, K. (2020) Stilling and recovery of the surface wind speed based on observations, reanalysis, and geostrophic wind theory over China from 1960 to 2017. *Journal of Climate*, 33(10), 3989–4008. https://doi.org/10.1175/JCLI-D-19-0281.1.